AD-A050 172 JOHNS HOPKINS UNIV LAUREL MD APPLIED PHYSICS LAB F/G 3/2
USE OF INTERPLANETARY RADIO SCINTILLATION POWER SPECTRA IN PRED--ETC(U)
OCT 77 E C ROELOF, B L GOTWOLS, D G MITCHELL N00017-72-C-4401
UNCLASSIFIED AFGL-TR-77-0244 NL

| OF |
AD
A050172

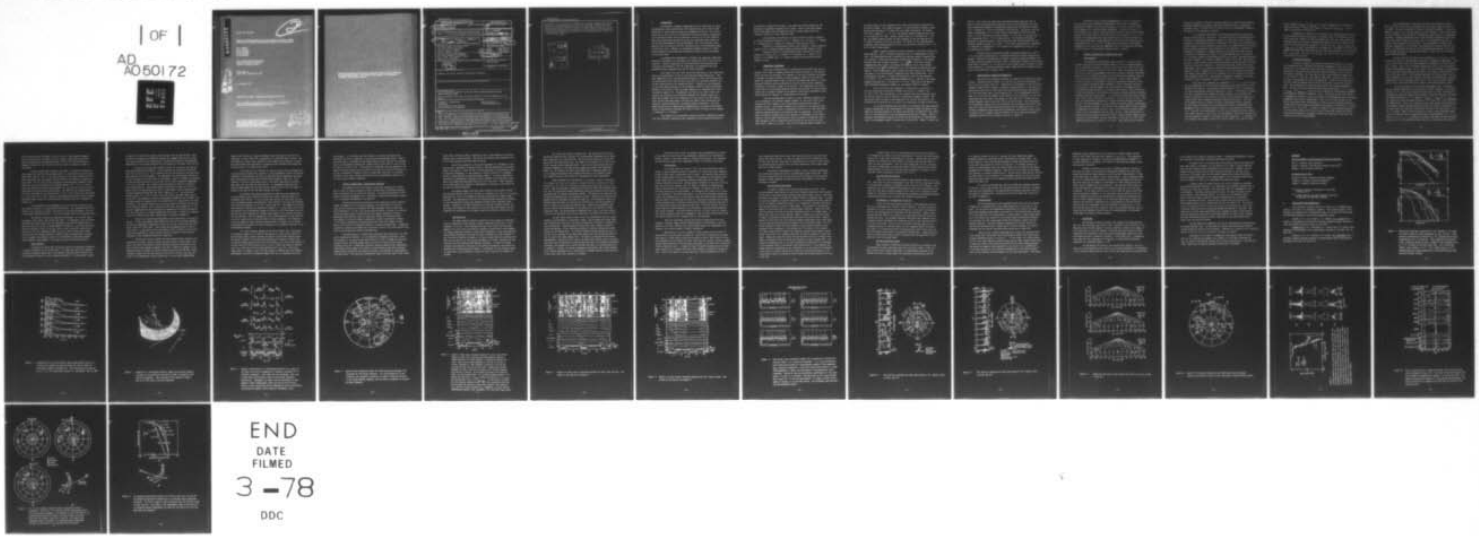

END
DATE
FILMED
3-78
DDC

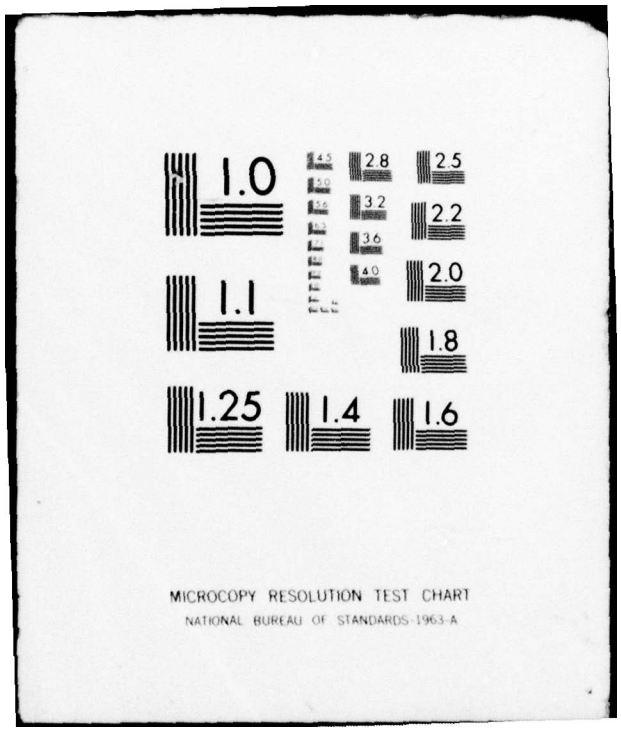
1.0
1.1
1.25
1.4
1.6
1.8
2.0
2.2
2.5
2.8
3.2
3.6
4.0
MICROCOPY RESOLUTION TEST CHART
NATIONAL BUREAU OF STANDARDS-1963-A

AFGL-TR-77-0244

# USE OF INTERPLANETARY RADIO SCINTILLATION POWER SPECTRA IN PREDICTING GEOMAGNETIC DISTURBANCES

E. C. Roelof
B. L. Gotwols
D. G. Mitchell
W. M. Cronyn
S. D. Shawhan

The Johns Hopkins University
Applied Physics Laboratory
Laurel, Marylnad 20810



Final Report
June 1976 - September 1977

31 October 1977



This research was supported by the Air Force In-House Laboratory Independent Research Fund.



AIR FORCE GEOPHYSICS LABORATORY
AIR FORCE SYSTEMS COMMAND
UNITED STATES AIR FORCE
HANSCOM AFB, MASSACHUSETTS 01731

Unclassified

SECURITY CLASSIFICATION OF THIS PAGE *(When Data Entered)*

**REPORT DOCUMENTATION PAGE**

READ INSTRUCTIONS BEFORE COMPLETING FORM

| | |
|---|---|
| 1. REPORT NUMBER: AFGL-TR-77-0244 | 2. GOVT ACCESSION NO. |
| 3. RECIPIENT'S CATALOG NUMBER | |
| 4. TITLE (and Subtitle): Use of Interplanetary Radio Scintillation Power Spectra in Predicting Geomagnetic Disturbances | 5. TYPE OF REPORT & PERIOD COVERED: Final rept. June 1976-September 1977 |
| | 6. PERFORMING ORG. REPORT NUMBER |
| 7. AUTHOR(s): E. C. Roelof, B. L. Gotwols, D. G. Mitchell, W. M. Cronyn and S. D. Shawhan | 8. CONTRACT OR GRANT NUMBER(s): MIPR [redacted] FY 7121760012 to Contract N00017-72-C-4401, Department of the Navy |
| 9. PERFORMING ORGANIZATION NAME AND ADDRESS: The Johns Hopkins University, Applied Physics Laboratory, Laurel, Maryland 20810 | 10. PROGRAM ELEMENT, PROJECT, TASK AREA & WORK UNIT NUMBERS: 61101F, ILIR6IAA, 6I |
| 11. CONTROLLING OFFICE NAME AND ADDRESS: Air Force Geophysics Laboratory, Hanscom AFB, Massachusetts 01731, Monitor/D.F. Smart/PHG | 12. REPORT DATE: 31 October 1977 |
| | 13. NUMBER OF PAGES: 40 |
| 14. MONITORING AGENCY NAME & ADDRESS *(if different from Controlling Office)*: 42 p. | 15. SECURITY CLASS. *(of this report)*: Unclassified |
| | 15a. DECLASSIFICATION/DOWNGRADING SCHEDULE |

16. DISTRIBUTION STATEMENT *(of this Report)*

Approved for public release; distribution unlimited.

17. DISTRIBUTION STATEMENT *(of the abstract entered in Block 20, if different from Report)*

18. SUPPLEMENTARY NOTES

This research was supported by the Air Force In-House Laboratory Independent Research Fund.

Work performed as Task ZJ20 of contract N00017-72-C-4401, Department of the Navy.

19. KEY WORDS *(Continue on reverse side if necessary and identify by block number)*

Geomagnetic disturbances
Prediction
Interplanetary scintillations
Solar-terrestrial disturbance
Radio astronomy
Interplanetary medium

20. ABSTRACT *(Continue on reverse side if necessary and identify by block number)*

An investigation of the feasibility of using interplanetary scintillations (IPS) of cosmic radio sources for prediction of geomagnetic disturbances has been carried out based on observations taken May-December 1974 and May-August 1976. The 1974 observations were taken with the University of Iowa COCOA-Cross array at 34.3 MHz located at Clark Lake Radio Observatory near Borrego Springs, California and synoptic data on 33 sources were reduced to yield scintillation index (band-pass integrated IPS power) for each source. In 1976, COCOA-Cross

DD FORM 1 JAN 73 1473 EDITION OF 1 NOV 65 IS OBSOLETE

Unclassified

SECURITY CLASSIFICATION OF THIS PAGE *(When Data Entered)*

031650

observations at 34.3 MHz were supplemented by 38 MHz observations from the University of Maryland TPT array, also at Clark Lake, and the high time resolution data were reduced to obtain IPS power spectra from 0.1 to 3 Hz. From detailed analyses of both data sets, we conclude that IPS prediction of the onset of geomagnetic disturbances may be feasible with a lead time of about one day.

## 1. INTRODUCTION

We proposed a 15-month investigation of the feasibility of using interplanetary radio scintillation (IPS) observations at 34.3 MHz for the prediction of solar particle events and geomagnetic activity. *Our overall conclusion is that 24-hour IPS prediction of solar-terrestrial disturbances may be feasible within certain constraints intrinsic to the IPS technique.* Since the observations upon which we base our conclusions were limited to two periods, May-December 1974 and May-August 1976, the inferences drawn directly from our data are strictly applicable only to the descending phase of the solar cycle. However, our theoretical analysis allows us to make some evaluation of IPS prediction feasibility during the rise and maximum of the solar cycle.

A promising new development is evidence that important additional prediction information is contained in the functional form of the IPS *power spectrum*. Previous comparisons of IPS observations with interplanetary structure relied mainly on the IPS index which is essentially the total normalized power integrated over the IPS power spectrum.

This report will not cover the actual operations of the COCOA-Cross array by the University of Iowa at the Clark Lake Radio Observatory. They were summarized in our Interim Scientific Report (1 April 1976-31 March 1977) on Contract NPP-75-157 from the Air Force Office of Scientific Research who are also supporting our IPS prediction effort. Progress on the up-grading of the array, made necessary by the flooding of Clark Dry Lake by Hurricane Kathleen in the Fall of 1976, was again delayed by an unprecedented 15-inch flooding in August 1977. Consequently, the bulk of our effort under this contract was devoted to the scientific analysis IPS synoptic index data taken May-December 1974 by the University of Iowa, and to the IPS synoptic power spectra taken May-August 1976 with the digital data acquisition and reduction systems developed at the Applied Physics Laboratory. The 1976 COCOA-Cross data were significantly supplemented by concurrent observations using the University of Maryland TPT array at CLRO, for which we are indebted to Professor W. C. Erickson.

The results of the scientific analysis provided considerable insight into the prediction problem and were submitted as three separate articles to

the *Journal of Geophysical Research*. All three have been refereed and the revisions are pending acceptance by the editor. Many of the ideas summarized in this Report are discussed more fully in these papers which are currently available in their preprint form.

*Interplanetary Scintillation at Large Elongation Angles: Response to Solar Wind Density Structure*, by F. T. Erskine, W. M. Cronyn, S. D. Shawhan, E. C. Roelof and B. L. Gotwols (University of Iowa Preprint 77-24).

*Analysis of Interplanetary Scintillation Spectra at Large Elongation Angles*, by D. G. Mitchell (Applied Physics Laboratory/JHU Preprint 77-07).

*Synoptic Analysis of Interplanetary Radio Scintillation Spectra Observed at 34 MHz*, by B. L. Gotwols, D. G. Mitchell, E. C. Roelof, W. M. Cronyn, S. D. Shawhan and W. C. Erickson (Applied Physics Laboratory/JHU Preprint 77-13).

## 2. THEORETICAL BACKGROUND

One of the justifications for constructing the COCOA-Cross array to operate at 34.3 MHz, a frequency lower than usually utilized for IPS observations, was that the increased IPS response at the lower frequency would make it possible to observe sources at large elongation angles ($\epsilon$) from the sun (where IPS response falls off due to both the decreased mean density of interplanetary electrons and the reduction in the solar wind velocity component transverse to the line of sight to the source). The expectation was to have a dense grid of scintillating sources covering the sky above the radio horizon (except for the region occupied by the galactic plane where interstellar scattering reduces the response to interplanetary scattering).

The main disadvantage in going to a lower observing frequency lies in the increase in the apparent angular diameter of the source, due to the increase with wave length of both interstellar scattering and extent of extended sources. The apparent angular source diameter is an important parameter in IPS prediction, since it determines from how far out into the interplanetary medium detectable scintillation power is generated. To be more exact, in weak-scattering theory the frequency ($\nu$) dependence of the contribution to the IPS power spectrum $dP(\nu)$ from an interval dL along the line of sight contains a source visibility function which we may take in the form $\exp(-\nu^2/\nu_S^2)$, where $\nu_S = V_\perp/\pi\theta L$. Here $\theta$ is the apparent angular diameter of

the source and $V_\perp$ is the component of the solar wind velocity transverse to the line of sight. For a given frequency $\nu$ in the IPS power spectrum, contributions from distances $L > V_\perp/\pi\theta\nu$ will be strongly attenuated. We measure $P(\nu)$ over a range $0.1 < \nu < 1.5$ Hz, and apparent angular diameters are often $\geq$ 1 arc-second at 34.3 MHz. Using a typical value $V_\perp \simeq 400$ km/s and $\nu = 0.5$ Hz, the nominal region "probed" by this component of the IPS spectrum for a 1" source is within 0.35 AU of the earth. Of course, if the interplanetary turbulence were localized beyond 0.35 AU, it would still contribute at $\nu = 0.5$ Hz if it were strong enough.

There is another important process intrinsic to IPS which affects the power spectrum. This is "Fresnel filtering" and it is independent of source size. The scintillation power contributed by electron density irregularities at a distance L rises with decreasing scintillation frequency $\nu$, but becomes constant below the "Fresnel frequency" $\nu_f = V_\perp/\sqrt{\pi\lambda L}$. This occurs because irregularities whose scale sizes exceed the diameter of the first Fresnel interference zone $\sim\sqrt{\lambda L}$ are "filtered" out of the spectrum by destructive interference. Thus irregularities near the earth are less effective at contributing power at low scintillation frequencies than those further away. For a scintillation frequency $\nu$, Fresnel filtering will occur for all distances $L < V_\perp^2/\pi\lambda\nu^2$. At $\lambda = 10$ m observing wavelength and $V_\perp = 400$ km/s, this gives Fresnel filtering for $L < 0.14$ AU for $\nu = 0.5$ Hz. Note that as one goes to lower observing frequencies (larger $\lambda$), the Fresnel effect is reduced.

These two effects were combined in a theoretical calculation of the thin screen power spectrum by *Mitchell and Roelof (J. Geophys. Res., 81, 5071, 1976)*. The contribution at each frequency was then integrated using all screens along the line of sight for a spherically symmetric medium. The spectra are shown in Figure 1 and demonstrate the Fresnel flattening at low scintillation frequencies and the source size suppression at higher frequencies.

It is clear therefore that the form of the observed IPS power spectrum contains information on the distribution of turbulence within the medium, since these two filtering effects on the power spectrum must be weighted by the variation for the distribution of the turbulence along the line of sight. Even in a quiescent interplanetary medium, the turbulence distribution is a strong function of the elongation angle $\epsilon$ from the sun to the source. Figure 2, taken from

*Mitchell (1977)* shows the theoretical contribution dm/dL along the line of sight for the band-passed power spectrum m (0.1-1.5 Hz) observed at 34.3 MHz from a spherically symmetric interplanetary medium with the electron variance $< \delta N^2 >$ varying as $r^{-4}$ with the distance r from the sun. The curves cover the range of elongations $60° < \epsilon < 160°$ and were calculated for source angular sizes $\theta = 0.01"$ (effectively a point source), $\theta = 3.0"$ (not an uncommon size at low frequencies) and $\theta = 7.0"$ (a large source). The Fresnel filtering is apparent for small distances L, while the source size filtering restricts the quiescent medium response to $\leq 0.5$ AU. At 34.3 MHz, scintillation is depressed or "quenched" at elongations $\epsilon < 40°$ because the scattering is strong due to the high electron density.

Although these calculations assumed a quiescent medium with $< \delta N^2 > \propto r^{-4}$, they can be generalized to a disturbed medium with locally enhanced turbulence. Mitchell's calculations for Figure 2 actually divided the medium into 20 slabs, and the locations of slabs 7 and 13 (indicated on Figure 2) are plotted along lines of sight at $\epsilon = 60°$ and 120° in the ecliptic plane in Figure 3, along with a sketch of a corotating turbulent region (shown fixed for sequential position of the earth every two days, a-d).

## 3. IMPLICATIONS OF THEORY FOR PREDICTION

We now have the essential concepts to interpret the COCOA-Cross observations. Referring back to Figure 2, we see that the bulk of the response of the 3" source is within slabs 1-7. Therefore for the geometry of the *corotating* turbulent region shown in Figure 3, enhanced scintillation at $\epsilon = 60°$ would be expected not more than 1-2 days before the corotating turbulence reached earth (c), and would cease about a day afterwards (b). No IPS enhancement would be seen at $\epsilon = 120°$ much in advance of the arrival of the turbulence (c), but the enhancement may last about a day longer (b) than that at 60° (unless the turbulence weakens outside the earth's orbit, as it well may). Most interplanetary disturbances during 1974-6 were recurrent and corotating, and we shall show below that these anticipated patterns occurred in the COCOA-Cross data. For radially propagating flare-associated disturbances, the response pattern would be similar, but of somewhat shorter duration, as can be seen by sketching an expanding spherical shell centered on the sun on Figure 3.

The theory tells us that the enhancement of *total scintillation power* is not the sole predictor available for the arrival of turbulence. Referring to Figure 1, we see that the *shape of the power spectrum* itself will change as the turbulent region approaches. For the $\frac{1}{2}$" source at $\epsilon$ = 60° in Figure 1b, it may be seen that the contribution from the more distant regions is *narrower* (due to the finite source size filtering $\nu > \nu_s \propto L^{-1}$), whereas the contributions from the closer region is *broader* (because the source size filtering is less important but the Fresnel filtering flattens the spectrum for $\nu < \nu_f \propto L^{-\frac{1}{2}}$). We have found this spectral broadening diagnostic in the data, and its importance lies in the additional information on *distance* to the turbulent region which it contains.

## 4. SYNOPTIC OBSERVATIONS: SCINTILLATION INDEX

### Data Analysis

The normalized scintillation index curves for a cluster of six sources covering an ecliptic latitude range of 9° and a longitude range of 57° are displayed in Figure 4. Over the time period 1974, days 231 to 296, this cluster was west of the sun. IMP-7 and 8 (near the Earth) solar wind density and velocity measurements (from the Los Alamos Scientific Laboratory detectors), the planetary $A_p$ index and the inferred interplanetary magnetic field polarity at the Earth are also provided. There is good temporal agreement between the occurrence of density enhancements (which are often, but not always, associated with the magnetic sector boundaries and which are followed by velocity peaks), and the occurrence of increases in the scintillation index for each of the sources individually. This correlation is expected because of the increase in scattering associated with the density increase along the line of sight. *The density-associated IPS index enhancements precede large increases in geomagnetic activity ($A_p$) by 1-2 days.* However, the quantitative correlation of index response from source-to-source varies. For the enhancement on days 256-259 all sources exhibit approximately the same increase in index. For days 231-234, however 3C68.2 barely responds in comparison to the other sources. Also, 3C125 and 3C153 increase significantly less on days 285-289 than the other sources. These observations of distinct source-to-source differences within a source cluster suggest spatial variations in the electron density turbulence on the scale of 2-10° and/or temporal variations on a scale of 3-16 hours. This scale size for density

structure is similar to velocity structure deduced for the solar wind velocity difference between two spatially separated satellites where a longitudinal coherence time of ~ 18 hours (10°) is found, as well as significant changes on the scale of a few degrees in latitude.

It is apparent from Figure 4 that missing observations obscure the pattern over the sky on a given day. A further difficulty is encountered when we desire to intercompare different sources on a given day; how are the IPS responses of different sources to be normalized? In Figure 4 the normalization to peak values is really arbitrary, since there is no assurance that each source line-of-sight contained the same turbulence on the peak days. Therefore we developed a non-parametric ranking scheme and also grouped adjacent sources in clusters (to minimize the effects of missing observations). We selected 45 of the most reliable scintillating sources for a source "clustering analysis". As shown in Figure 5, we chose 10 regions or "boxes" in the sky, each containing up to 8 radio sources, with the sources spaced no more than about 30° from any other source in the same box. The 10 sky boxes span nearly all ecliptic longitudes. Most of the boxes are centered at mid-northern ecliptic latitudes (from 20° to 50°). However, Box 5 is just south of the ecliptic, while Box 3 (the single source 3C161) is at -29° latitude. Box 9 is centered at a rather high latitude of about 70°. The method of assigning a weighted IPS response to each box ($Q_i$) is described in detail by *Erskine et al. (1977)*.

With the set of weighted box responses $Q_i$ ( i = 1, ..., 10) for each day of observations, we can now study the general large scale pattern of scintillation over the sky. One graphical representation of the $Q_i$ is given for the three observational periods in Figures 6, 7 and 8. Four levels of shading are used in Figures 6-8 to display the high, moderate, low or missing IPS activity estimates for each sky box, each day, with the darkest shading indicating "high", and no shading indicating "missing observation". The boxes are arranged from top to bottom in order of decreasing ecliptic longitude. At the bottoms of Figures 6-8 are displayed correlative interplanetary and geomagnetic data in a format similar to Figure 4 (see captions for Figures 6-8). The solar wind measurements are from the Los Alamos Scientific Laboratory (LASL) detector on IMP 7 and 8, and the magnetic field from the University of Iowa plasma wave search coil detector on IMP-8 spacecraft. In addition, we have computed the average "all-sky IPS acticity index", $\langle Q \rangle$, over all boxes.

We also compute $\langle Q \rangle_{east}$ and $\langle Q \rangle_{west}$ for each day, using only the eastern and western sky boxes. We show $\langle Q \rangle$, $\langle Q \rangle_{east}$, $\langle Q \rangle_{west}$ and $\langle Q \rangle_{high\ lat.} = Q_9$ vs time at the centers of Figures 6-8.

Examination of Figures 6-8 for evidence of a spatial-temporal pattern of IPS activity reveals the presence of vertical bands of occasional very low IPS acticity and "events" of high and moderate IPS activity. These event bands encompass nearly all ecliptic longitudes and appear to be most prominent near times of solar wind density increases. The plots of $\langle Q \rangle$, $\langle Q \rangle_{east}$, $\langle Q \rangle_{west}$ and $\langle Q \rangle_{high\ lat.}$ all peak at approximately the same time. The peaks of IPS activity appear to coincide well with peaks in solar wind proton density, and for the most part, $|B_{xy}|$ also. *The peaks in geomagnetic $A_p$ occur several days later than the peaks in IPS activity.*

Correlation Analysis

In order to examine the temporal relationship between the 34.3 MHz IPS enhancements and correlative ground-based geomagnetic, solar disc observations, and *in situ* spacecraft solar wind data, Erksine, in his dissertation, performed a time series cross-correlation analysis between $< Q(t) >$ and the correlative variables. The data base for this cross-correlation spans 1974, t = day 150 to t = day 362. The range of time shift used is $-10 \text{ days} \leq \tau \leq 159 \text{ days}$, corresponding to 75% of the data base. $< Q(t) >$ is the all-sky IPS activity index as described earlier and $\overline{Q}$ is the mean $< Q(t) >$ over the data base. The correlation has been performed against the following parameters X(t): all-sky IPS activity measure itself (auto-correlation) $< Q >$, $< Q >_{east}$, $< Q >_{west}$, $< Q >_{high\ lat.}$, solar wind proton density N, interplanetary magnetic field magnitude (ecliptic component) $|B_{xy}|$, solar wind proton bulk velocity V, geomagnetic planetary A index, occurrences of interplanetary sector crossings, geomagnetic storm sudden commencements, Type II and IV radio bursts (on the eastern and western solar hemispheres), as well as central meridian passage of coronal "hole" western edges as estimated from Figure 3 of *Hansen et al. (Planet. Space Sci., 24, 381, 1976)*. In order to compute a cross-correlation function for the discrete events (SSC's Type II and IV bursts and coronal hole CMP's), each event was assigned a triangular time profile centered on that date with a width of one day at half-maximum.

Six representative correlation functions are presented in Figure 9. Above each plot of $r(\tau)$ we have indicated the time shifts (days) for most of the peaks. The value of maximum correlation coefficient nearest $\tau = 0$ and the number of points, N, in the time series are also indicated. The inclined lines are 99% confidence limit estimates (assuming each measurement is an independent estimate). Missing observations due to radio frequency interference and telescope "down time" account for the fact that N is considerably less than the number of days spanned by the data base. We also summarize in Table 1 the essential parameters of all thirteen cross-correlation functions which we computed: the amplitudes and lags of the correlation peaks nearest to zero lag, and "average" lag which is the mean lag (modulo 27 days) over all the identifiable recurrence peaks.

We note that 99% confidence limit estimates of $r = 0.21$ for $n = 135$ assume that each day's observation constitutes an independent measurement. This is not true for IPS, solar wind and geomagnetic disturbances in which "events" last $\sim 3$ days. This is the well-known conservation effect in the statistical analysis of geomagnetic data. The net result is that the number of "independent" points will then be approximately one-third of the number of observations, so that the 99% limit for $n \simeq 135$ (although applicable to discrete events such as sector boundaries, SSC's, radio bursts, and coronal hole edge CMP's), should be interpreted as a 90% confidence limit with $n \simeq 45$ for the persistent enhancements of IPS, solar wind velocity and density, IMF intensity and $A_p$ index.

We see from Figure 9 that the IPS enhancements recur consistently over the interval spanned by the time shifts (5 solar rotations). The autocorrelation of $< Q >$ has a mean recurrence period of $28 \pm 2$ days, verifying our interpretation that the dominant IPS structure during this period is corotating. The cross-correlations of $< Q >$ against $< Q >_{east}$, $< Q >_{west}$ and $< Q >_{high\ lat.}$ (not shown) give mean recurrence periods of $27 \pm 2$ days, $28 \pm 2$ days and $27 \pm 1$ day respectively. There is no significant time shift between the correlations with eastern, western and high latitude sources (to within an uncertainty of 1-2 days), and the correlation coefficients in Table 1 are quite high ( $> 0.76$ for $\tau = 0$ days). Many of the correlations in Figure 9 show subsidiary peaks located 11-15 days from the main peaks which are approximately at $\tau = k \cdot 27$ days, $k = 0, 1, 2, \ldots, 5$, although they usually fall below the 99% confidence limit for $k \geq 2$. The subsidiary peaks (which are occasionally bifurcated) in

the correlation plots of Figure 9 are the result of the somewhat asymmetric solar wind two-sector structure in 1974. Computer simulations have shown that the amplitude of the subsidiary peak in $r(\tau)$ is far more sensitive to changes of spacing of the two-sector structure than to changes in height of the maxima.

Further examination of Figure 9 and Table 1 confirms our impression from Figures 6-8 that the IPS acticity index $< Q >$ correlates better with solar wind proton density, $r(0) = 0.56$, than with any of the other correlative parameters examined, and that density and IPS activity are evidently in phase with each other. IPS activity is also in phase with interplanetary magnetic field magnitude, but the correlation is noticeably smaller $r(0) = 0.37$. As can be seen from Figures 6-8, most large increases in $| B_{xy} |$ are the result of density compressions in stream-stream interactions. The IPS activity anticorrelates well with solar wind proton bulk velocity, $r(-2) = -0.52$, as well as correlating at a later lag $r(+3) = 0.38$. These are the normal lags between velocity minima preceding density peaks and velocity maxima following them, as is apparent in Figures 6-8.

The correlations with geomagnetic activity are also consistent with the nominal structure of stream-stream interactions. The correlation with SSC's peaks at zero lag while $A_p$ peaks a day later (as the storm develops), but with a correlation coefficient $r(+1) = 0.43$ that is higher than for the discrete SSC's.

The weakest correlations obtained were between $< Q >$ and IMF sector crossings, radio bursts, and coronal hole CMP's. In appearance, the correlation functions are rather similar and are marginally statistically significant, so only the result for sector crossings appears in Figure 9. The sector crossings would be expected to peak at zero lag, due to their statistical associations with SSC's, but the correlation peaks for Type II and IV bursts and coronal holes are not well enough defined to justify further interpretation, although in our judgement the dominant class of IPS disturbances during May-December 1974 exhibited a high degree of recurrence and were not flare-associated.

Event Analysis

We pointed out above that the density events are sometimes preceded by a trough of moderate and low IPS activity. It seems that there was a comparatively non-turbulent region west of the density structure which allowed it to be defined more clearly by line-of-sight measurements. Thr trough most evident

in Figure 6 is that in the eastern sources (boxes 5-8) on days 156-159. Even though we are limited by incomplete coverage and somewhat noisier data during this initial period of our observations, the data still permit a more detailed examination of the cluster analysis for the duration of the event, days 156-163.

Plotted in the left-hand column of Figure 10 are the $Q_1$ for each day when observations were available. Since 3C161 was not observed at this time, there are no data for $Q_3$. At the head and foot of the column are the LASL solar wind densities (3-hour averages). The orientation of the sky-boxes relative to the sun is shown in the right half of the figure. Boxes 5-7 display low Q-values on days 156-158 while Box 4 is low on day 157 but shows a moderate enhancement (Q = 0.9) on day 158. Box 4 would be the first group of sources to detect a corotating structure. The eastern onset of the event is clear on day 159 in Boxes 5 and 6 (no observations for Box 4), while Boxes 7 and 8 (covering solar ecliptic longitude between 90° and 150°), remain at Q = 0. The solar wind density peaks at N = 25 $cm^{-3}$ early on day 161, and an "all-sky" event occurs on day 162. The enhanced Q-indices are sustained through day 163 in Boxes 7-10 (viewing sources at longitude west of the direction of a stream front at earth), while Box 1, the closest western box to the sun, shows an increase on that day. On the contrary, Boxes 2 and 4, just east of the sun, have dropped to Q = 0 on day 163, suggesting that the disturbance now appearing in the west has passed over the earth and is no longer visible east of the sun. A sketch of a density structure consistent with these observations is offered in Figure 10.

There is an interesting enhancement in the western Box 1 on days 156 and 157. At that time McMath plage region 12972 was in the western hemisphere on the sun, producing an importance 1B flare on day 155.0 (S14, W13) and a 3B flare on day 157.7 (S16, W48). Both flares had accompanying Type II and IV radio bursts. It may well be that the sources in Box 1 (which is at low latitude) were responding to plasma ejected from the vicinity of MPR 12976 (as indicated on the accompanying sketch in Figure 10).

We shall now turn to another IPS event wherein almost identical circumstances are found. However, since this second event occurred half a year later, our source distribution favored detailed analysis of structure to the west of Earth, with minimal coverage to the east. Figure 11 presents, in an identical format to Figure 10, the IPS density event of days 330-338. Source clusters in Boxes 6-8 now view sources to the west of the sun, and they all detect an IPS enhancement on days 332 and 333. At this time, McMath plage

region 13343 was west of central meridian, later producing on day 334.3 an importance -B flare (N03, W52) accompanied by an isolated Type II burst. The confirmation by three source clusters of the western event leads us to interpret this western IPS enhancement as plasma emitted from MPR 13343 during its activity prior to the flare on day 334.3.

If we now turn our attention to the sole source cluster viewing east at mid-latitudes (sky-box 10), there is a clear enhancement on days 333 and 334 following low scintillation activity on days 330-332 and leading to sustained high scintillation on days 335-337 which drops abruptly on day 338. This sequence of activity corresponds nicely to the solar wind density structure that swept over the earth on days 335-337. It presumably would have been detected approaching from the east on days 333 and 334 and could no longer be viewed to the east on day 338 after passing the earth.

The western and eastern signatures are made even more significant by the extremely quiet conditions in the other source clusters (Boxes 1-5) throughout days 330-334. It is not until days 336 and 337 that these sources, all at elongation angles exceeding 90°, fully respond to the solar wind density structure which peaked at $N = 51\ cm^{-3}$ late on day 336. The suggested interplanetary density structures are sketched in Figure 11. It seems clear that it was only because the interplanetary medium to the west of the corotating structure had been so quiet (examine the "trough" which stands out so clearly in Figure 8 for days 330-334), that the signatures of the corotating event in the east and the active region event in the west were so easily separable. One therefore is led to regard the less ordered structures seen in Figures 6-8 as perhaps reflecting more accurately the usual complexity of the density structure of the interplanetary medium.

As a final detailed example of IPS events viewed over a wide range of elongation angles, let us look at the response of each source observed on day 332 (the western event) and days 336 and 337 (the all-sky density event). We present in Figure 12 an equal-area projection of the sky as viewed from the earth looking toward the sun. The IPS response $q_j$ for each source appears as an open circle for low activity ($0 \leq q_j < 2/3$), a cross for moderate activity ($2/3 \leq q_j \leq 4/3$) and a star for high activity ($4/3 < q_j \leq 2$). The active region event is evident on day 332 (even though it involves only the moderate enhancements expected at elongation angles $\leq 60°$ due to quenching by strong

scattering). It is obvious that this pattern of activity would have gone undetected had not the remainder of the sky been exceptionally quiet. Nearly the entire sky is in medium or high scintillation on days 336 and 337, although there is a perceptible tendency for lesser activity from -120° to -180° on 336, but from 0° to 120° on 337. This pattern is consistent with the maximum of the density structure passing over the earth on day 336, as we noted from Figure 11. In fact, comparison of Figures 11 and 12 should make clear why it is usually necessary to use source cluster analysis when the interplanetary medium is in its more usually complex condition.

## 5. SYNOPTIC OBSERVATIONS: SCINTILLATION SPECTRUM

The analysis of the 1974 synoptic index data confirmed our opinion that it would be highly desirable to have the additional information available which is contained in the actual IPS spectrum. We therefore analyzed our 1976 synoptic spectral measurements for a signature of approaching turbulent regions, i.e., a systematic broadening of the spectra.

Observations from the University of Iowa COCOA-Cross radio telescope during the summer of 1976 (17 May-25 August) were supplemented by observations on the University of Maryland TPT radio telescope, also at Clark Lake Radio Observatory. Of the ~ 151 sources observed daily, a subset of 41 sources proved favorable enough in location, flux and angular diameter to produce measureable scintillation power at least once during the observing period. This subset of sources is shown in geocentric ecliptic coordinates in Figure 13. Of these, 9 consistently yielded spectra with sufficient signal-to-noise ratios to be used in the synoptic analysis of spectra presented here. Reasonably continuous coverage was obtained for the period 9 June-17 July (days 166-199) and this is the period which will be discussed here.

The COCOA-Cross is a pencil beam instrument which operates at 34.3 MHz with a bandwidth of 500 kHz. It is electrically steerable north-south, while the rotation of the earth causes radio sources to "drift" through the east-west antenna pattern, providing usable data on a source for about three minutes. Starting on day 183 a rudimentary east-west steering capability was implemented which allowed the antenna to be pointed to three discrete east-west pointings, symmetrically spaced about the central meridian, and separated by approximately two beam widths. This east-west steering was used for sources 3C48, 3C196, 3C216,

3C254, 3C273, 3C298 and 3C380, resulting in six to nine minutes of data each sidereal day for these sources. The latter four sources were observed at two of the three possible east-west beam positions.

The TPT was operated in the pencil beam mode at a frequency of 38.0 MHz and with a bandwidth of either 150 kHz or 800 kHz depending on the zenith angle of the source. Since the TPT is fully steerable in all directions (but in discrete increments), it was possible to track a source for an extended period of time centered on central meridian transit. A typical observation consisted of incrementally tracking a source (similar to the east-west tracking by the COCOA-Cross described above) for up to one hour. After allowance for the beam shape this results in approximately 25 minutes of data which can be used for spectral analysis.

The analog signals from both radio telescopes were passed through 4 pole low-pass filters (which were designed to eliminate the effects of aliasing), digitized at a rate of 10 samples per second, and stored on a digital tape recorder. The observations from the two radiotelescopes frequently overlapped in time and generally showed good agreement between their respective power spectra. Therefore, the small difference in observing frequency between the two arrays was ignored in the analysis and the two data sets merged into one composite set consisting of the highest quality observations from each array.

## Data Reduction

The power spectrum analysis consists of first taking out long-term trends by passing the data through a digital high-pass filter with a cutoff frequency of 0.02 Hz. These high-pass data are then broken into 256 point segments (25.6 sec) and a fast Fourier transform is performed on each segment. The average magnitude squared of each Fourier component is then calculated and corresponding components from each 256 point transform are added together to give the desired spectral estimates. On those sources which are observed more than once per day all of the spectral estimates are further combined into one composite spectral estimate with improved stability. In order to further increase the statistical stability of the spectral estimates, the spectra are smoothed with a Hanning spectral window. For example, for the spectrum shown in Figure 14a, which represents 9 minutes of data, there are 112 degrees of freedom.

Two curves are plotted in Figure 14a. The upper curve is the raw uncorrected spectrum which consists of a scintillation component plus a white noise component due to system noise. The actual data points are at the left hand end of each horizontal line. The sharp cut-off above 3 Hz is due to the 4 pole low-pass filter mentioned above. Since in our observations the scintillation component of the spectrum has always been found to be negligible above 2 Hz, we estimate the white noise amplitude by averaging across the 2 to 3 Hz range and subtract that estimate from each of the spectral points. This yields the lower curve which for convenience has been renormalized.

When displayed on a log-log plot, the spectra typically displayed a flat plateau from very low frequencies turning over into a power-law at high frequencies, the turn-over occurring at anywhere from less than 0.1 Hz up to 0.5 Hz. Both the turn-over frequency and the rate at which the spectrum turns over into the power-law provide information about the velocity of the scattering medium and its density turbulence profile. The slope of the power-law also provides information about the turbulence profile. Therefore, the spectra are parametrized by recording the power-law slope ($\alpha$), the frequency at which the smoothed spectrum drops to 3 dB below the plateau ($\nu_3$), and the frequency at which it drops to 6 dB below the plateau ($\nu_6$). These three parameters then serve as useful characterizations of the spectra for the analysis of large amounts of data. We are principally concerned with $\nu_3$ and $\nu_6$ in this report; $\alpha$ will not be discussed here, but was analyzed in the paper by *Mitchell (1977)*.

We have taken several steps to cast out observations that are contaminated by interference of terrestrial origin. The 10 sample per second high-pass filtered data from which the power spectrum was calculated is plotted for every observation. Having inspected similar plots for a number of cases of known interference, it was frequently possible to identify terrestrial interference in the observations. To further validate the measurements we plot 2.5 sec and 50 sec averages of the main beam response and the fluctuation power in the 0.1 and 1.5 Hz range (Figure 14b). The peak in scintillation power must approximately coincide with the peak in the main beam response, and on the fine time scale the fluctuations in scintillation power must be reasonably distributed throughout the passage of the source through the beam, or the observation will be rejected. Finally, the spectra themselves occasionally show strong harmonically related components due to interference, although usually in this case one of the other tests also confirms its presence.

With these strict tests, we estimate that approximately two percent of the remaining observations are unknowingly contaminated by interference. However, because of the large number of observations analyzed, the contaminated observations should have a negligible effect on the final conclusions.

Data Analysis

It has been shown by *Mitchell (1977)* that IPS observations taken at 34 MHz at large elongation cannot be modelled by a single thin phase changing screen on which most scintillation work is based. The question then arises as to what changes might occur in the shape of the spectrum as the dominant scattering region (due to the enhanced turbulence associated with a solar wind stream), approaches the earth. Having analyzed hundreds of spectra we can say that the form of the spectrum (not its height or breadth) is approximately similar when plotted on a log-log plot. However, the spectra tend to turn over more sharply as they get broader. We interpret this trend to be a result of the thickness of the scattering medium. In the weak scattering interpretation, the superposition of contributions along the line-of-sight deforms the spectral shape of the spectrum from that of a thin-screen spectrum and produces a final spectrum with a shallower slope and more gradual turn-over than any of the contributing thin-screen spectra would have. For broad spectra, the relatively near-earth medium dominates the scattering, producing an approximately thin screen spectrum. The narrow spectra are apt to be the result of scattering from an extended region (for elongations $> 60°$) in which contributions from the distant medium add low frequency power to the spectrum.

There are occasional spectra which differ significantly from the majority. The most common deviant spectra exhibit an enhancement at low frequencies ($\lesssim 0.2$ Hz), flatten into a well defined plateau at intermediate frequencies, and turn-over again at higher frequencies.

Daily values of $\nu_3$ for a number of radio sources for the period of days 166-199, 1976 are shown in Figure 15. We have not included the two component spectra in this figure, since they occurred on only a small number of days. For comparison we also display the solar wind velocity, density, and most proable thermal speed measured by the MIT plasma instrument on the IMP-7 and 8 spacecraft *(Solar Geophysical Data)*. A number of cases of spectral broadening can be seen, some of which are correlated with solar wind streams as revealed by spacecraft data. There is no reason to believe that any of these broadenings are due to

flare associated blast waves, since solar activity was at a very low level during this entire period. In fact, as reported in *Solar Geophysical Data*, for both June and July there were no observed Type II or Type IV radio bursts, no confirmed $H_\alpha$ flares greater than sub flare importance, and no high energy electron or proton events.

The spectral measurements in Figure 15 show a definite broadening both before and during the rise of the high speed stream of day 182. Since our data coverage was best for this event we will discuss it first and then comment on other prominent features for which, unfortunately, we had less continuous coverage.

Day 182 Solar Wind Stream

A period of enhanced IPS activity began late on day 181. This occurred several hours before the solar wind velocity measured at earth started to rise due to the approaching corotating high speed stream, and at a time when the solar wind density at earth had already reached an enhanced level. In order to study the temporal and spatial evolution of the scintillation power spectrum we plot in Figure 16 quantized values of $\nu_3$ in geocentric ecliptic coordinates with the sun located at the top of each panel. The sequence of observations begins at the sun and runs in a counterclockwise direction. Figure 16a shows that all sources for which we had data displayed spectra of average width. In Figure 16b, the first source observed, 3C196, continues this trend and shows no signs of detecting the approaching corotating solar wind stream. Approximately one half hour later the situation changes significantly when 3C216 shows a broad spectrum which reflects the approach of the oncoming stream. The different response of 3C196 and 3C216 implies a large spatial gradient in the strength of the turbulence of this stream out of the plane of the ecliptic. All other sources shown in Figure 16b displayed unusually broad spectra except 3C263.1 which had a two component spectrum, the second component of which was broad. Figure 16c shows the return of scintillation activity to normal; while 3C196 is broadened, 3C216 and 3C254 have returned to their average width. Confusing the simple picture of the event terminating as abruptly as it had begun is the enhanced width of the eastern radio source 3C270.1. This behavior may simply indicate a graininess in the turbulence out of the plane of the ecliptic. In any case it is clear from Figure 15 that the scintillation spectra of all other sources return to average or below average width approximately by the end of day 183.

Another aspect of the scintillation activity on day 182 which is not brought out in Figure 16 is the large number of usually non-scintillating sources (at 34 MHz) that scintillated on that day. Because they were rarely observed to scintillate we were unable to classify their spectra based on their own past performances. This "all-sky" enhancement of IPS in association with an enhancement in solar wind density (which precedes the velocity maximum) makes it clear that the event under discussion is similar to the "all-sky" events discussed by *Erskine et al. (1977)*.

Day 169 Solar Wind Stream

Solar wind proton density peaked at approximately 0600 hr UT on day 169. There were no radio observations on day 168. The only observation during a 24-hour period centered on 169/0600 is that of 4C+21.53 at 169/0940. This source did not show the expected broadening but due to its high ecliptic latitude (42°) and large elongation angle at this time (127°) it would be unwarranted to conclude that this one observation contradicts the enhanced spectral broadening associated with the solar wind stream described above.

Broadening of 3C48 Spectrum on Day 191

On day 191 the scintillation spectrum of 3C48 broadened almost as much as it had during the "all-sky" event of day 182. The solar wind data available to us had a large data gap which was not over until the middle of day 191 (at approximately the time when 3C48 was observed). Based on this limited data set there is no evidence of a high speed solar wind stream engulfing the earth. Any enhanced turbulence must have been confined to the northern ecliptic hemisphere at a distance no greater than several tenths of an AU above the earth. This out of the ecliptic turbulence gave rise to broadened spectra for 3C48 and 3C196, and two component spectra for 3C68.2 and 3C254. It is unfortunate that our near-ecliptic radio source 3C273 was not successfully observed due to terrestrial interference. Judging from the lack of a solar wind stream at earth we presume that the spectrum of 3C273 would have been of average width.

Day 197 Solar Wind Stream

Radio frequency interference severely limited our coverage of the scintillation activity associated with this solar wind stream. Since the well defined proton density enhancement is approximately centered on the middle of day 197, we might expect the associated scintillation activity

to be wholly confined to day 197. Sources 3C273 and 3C298 both exhibit broadened spectra but 3C196 and 3C270.1 had spectra of average width. The proton density at earth had already returned to normal when 3C196 (which was in the east) was observed at 20 hr UT on day 197. Its average response is therefore understandable since the line-of-sight did not intersect the denser, presumably more turbulent, material. Thus two out of the three sources which were expected to broaden actually did so. The one source which did not (3C270.1) may have failed to do so because of a latitudinal structure in the solar wind turbulence since 3C270.1 is at a higher ecliptic latitude than either 3C273 or 3C298 (see Figure 13).

It is also interesting that 3C273 and 3C298 were somewhat broadened on day 196. Since these sources were favorably located in the east it appears that they were responding to the approaching corotating stream more than one day before it reached earth. The spectra for 3C273 on days 195, 196 and 197 are shown in Figure 17.

Interpretation

We have established in the preceding section that the IPS spectrum broadens as a corotating solar wind stream sweeps over or very near to the earth. We can discuss this phenomenon qualitatively in terms of the usual thin phase changing screen model as the source of the scintillations. *Mitchell (1977)* has shown that IPS observations at 34 MHz require a thick screen model, but if the effects are similar for the screens whose contributions dominate the spectrum, the thin screen model should give adequate insight into the spectral behavior. The high frequency dependence of our best spectra for 3C48 can be characterized by a power-law so we shall interpret our results assuming that the spatial turbulence spectrum was also a power law.

There are two possible mechanisms which control the spectral width from a given thin screen which can be discussed in terms of the theoretical concepts presented earlier in Section 1. In the first, for a point source, or for a very small apparent diameter source such as 3C48, Fresnel diffraction "filters out" much of the energy associated with the large scale turbulence and causes the temporal power spectrum to turn over at $\nu_f \propto V_\perp/\sqrt{Z}$ where $V_\perp$ is the bulk velocity of the turbulence perpendicular to the line-of-sight, and Z is the distance from the observer to the scattering region. The second

mechanism (finite angular size cutoff) applies to larger diameter sources such as 3C273, where the turn-over frequency is $\nu_S \propto V_\perp/Z$. Thus regardless of which mechanism is dominant, increasing the perpendicular component of the bulk velocity or decreasing the distance to the scattering region causes the spectrum to broaden.

In order to settle the question of whether distance, velocity, or both were the cause of the observed broadening we examined the solar wind velocity and spectral data obtained by multi-size IPS observations at 74 MHz by the UCSD group *(J. Harmon, Private Communication)*. Due to randomly spaced gaps in our observations and limited overlap in the available data sets, we were left with only a sequence of observations of 3C48 centered on day 182 which could be compared at both frequencies. The velocity derived from the 74 MHz observations of 3C48 showed no increase on day 182 or for two days thereafter. On the other hand both the 34 and 74 MHz IPS spectra were anomalously broadened, leading us to the conclusion that at least for this one well documented case and for the assumption of a power-law turbulence spectrum it is the changing distance to the turbulent region which controls the width of the spectrum. Considering the all-sky nature of the day 182 IPS activity this is in agreement with the conclusion of *Erskine et al. (1977)* that all-sky events are not a response solely to increased velocity, but are associated with enhanced turbulence near the leading edge of a high speed stream where the density is also enhanced.

## 6. CONCLUSIONS

Our analysis of the May-December 1974 synoptic IPS index data has led us to the conclusion that source sizes, typically $\geq$ one arc-second at 34.3 MHz,often limit the IPS response from those sources to within a few tenths of an AU from earth if there is enhanced turbulence with the vicinity of earth. Comparison with spacecraft solar wind density measurements shows that local high densities lead to strong IPS response. On the other hand, if densities near earth are low, there may be IPS response to more distant turbulence, especially for elongation angles $\epsilon < 90°$.

Our May-August 1976 synoptic IPS spectrum data indicate that the width of the scintillation power spectrum can provide information on the *distance* of the turbulent region from the earth, within the range which can be probed due

to the finite source spectral filtering effect. Progressive broadening of spectra were observed as corotating turbulence approached the earth.

In neither 1974 or 1976 were there sufficiently strong flare-associated solar wind shocks to determine the IPS response at 34.3 MHz to these structures which are more common during the maximum of the solar cycle. However, the pronounced recurrent solar wind structure during the decline of the last cycle allowed us to establish that the IPS reponse signature was clearly associated with the enhanced densities in the leading edges of the corotating streams which should be similar to those in an expanding flare-associated shock.

A nominal range of several tenths of an AU for probing the interplanetary medium using UPS observed at 34.3 MHz means that reliable prediction may be feasible if a lead time of about a day before the *onset* of a geomagnetic storm is acceptable. This time interval should be about the same for either corotating streams or flare-produced shocks. Of course, it is necessary to have sources near the ecliptic plane for positive identification of turbulence about to envelope the earth. One must bear in mind that the distribution of scintillating sources is not uniform over the sky (see Figure 13). The orientation of the galactic plane is such that as seen from California the source grid is densest toward the east in Spring and Summer and sparsest in the Fall. The sensitivity to flare shock disturbances will likewise be least in early Winter therefore prediction reliability will depend somewhat on time of year, although the least favorable periods for either corotating or flare-associated disturbances last less than two months.

One-day prediction capability can only be established with high quality, continuous synoptic data. We were unable to obtain data meeting these specifications during the period of this contract. Therefore our results are not definitive; however we believe that we can draw the following conclusions:

*Prediction of the onset of geomagnetic disturbances using IPS observations at 34.3 MHz does not appear to be reliable for lead times exceeding one day, but there is preliminary evidence that it may be feasible for < one-day lead times, especially if synoptic spectral observations are utilized.*

## 7. PERSONNEL

The Johns Hopkins University/Applied Physics Laboratory

Bruce L. Gotwols, Senior Physicist
Donald G. Mitchell, Post-Doctoral Research Associate(1)
Edmond C. Roelof, Senior Physicist

The University of Iowa

Willard M. Cronyn, Associate Research Scientist
Frederick T. Erskine, Doctoral Candidate(2)
Stanley D. Shawhan, Associate Professor

(1) Research Associate, University of Iowa after 1 February 1977

(2) Current address: Astronomy Program, University of Maryland, College Park, Maryland

## 8. PUBLICATIONS AND PRESENTATIONS

Three articles, listed at the end of Section 1, are pending publication in the *Journal of Geophysical Research*. The following papers on this research were presented by the underlined author at the Fall 1976 and Spring 1977 National Meetings of the American Geophysical Union:

Erskine, F. T., W. M. Cronyn, S. D. Shawhan, E. C. Roelof and B. L. Gotwols, Interplanetary scintillation at large elongation angles: Response to solar wind density structure, *EOS, 57*, 998, 1976.

Gotwols, B. L., D. G. Mitchell, E. C. Roelof and W. M. Cronyn, Power spectra of interplanetary radio scintillations observed at 34.3 MHz, *EOS, 57*, 999, 1976.

Gotwols, B. L., E. C. Roelof, W. M. Cronyn, D. G. Mitchell and W. C. Erickson, Synoptic spectral analysis of interplanetary radio scintillations May-August 1976, *EOS, 58*, 485, 1977.

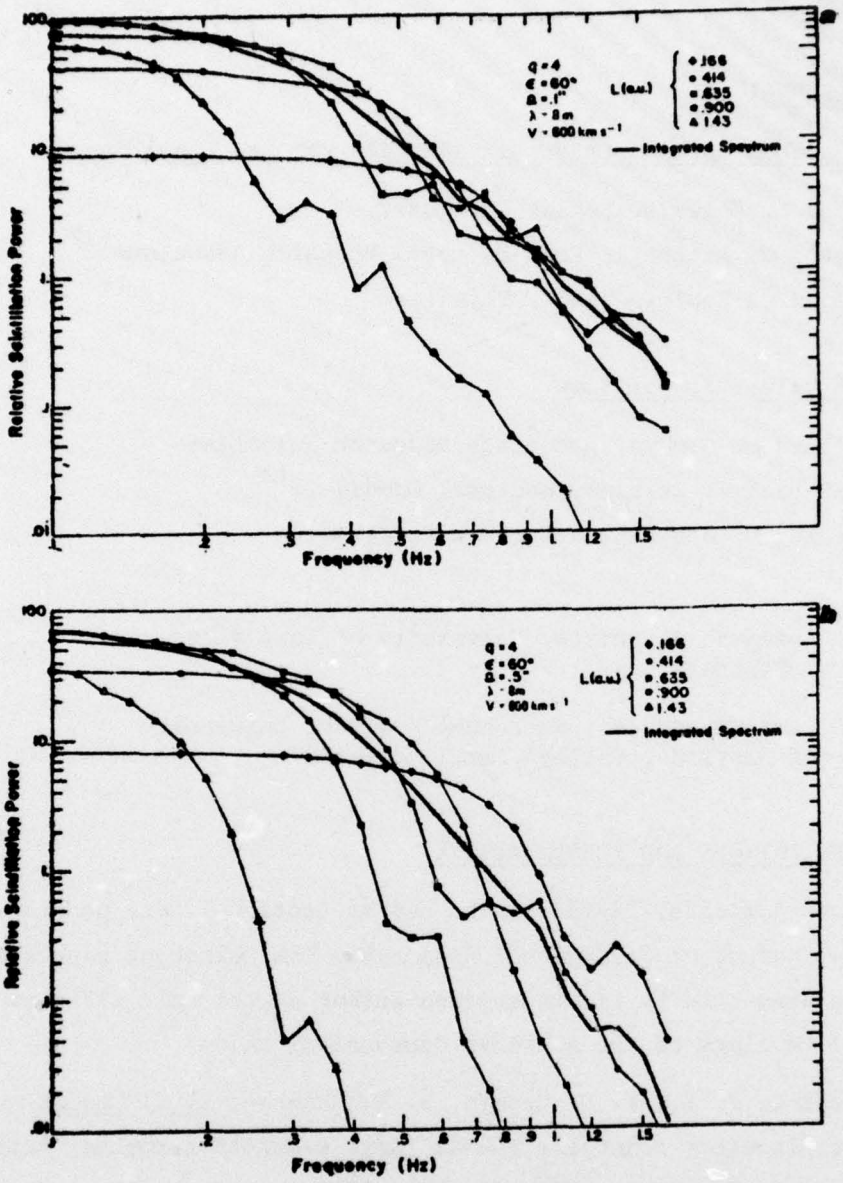


**Figure 1** Thin-screen spectrums calculated for five distances L (out along the line of sight) by using expansions $J_I$, $J_{II}$, and $J_{III}$. Their relative normalization is given by $F_o \propto r^{-4}$, although the absolute normalization of $F_o$ is arbitrary. The integrated scintillation power, integrated along the line of sight for each frequency with $F_o \propto r^{-4}$, is given by the heavy solid line. (a) A relatively "small" source radius $\Omega = 0.1"$. (b) A larger source $\Omega = 0.5"$, demonstrating the strong suppression of the high-frequency power from more distant screens.

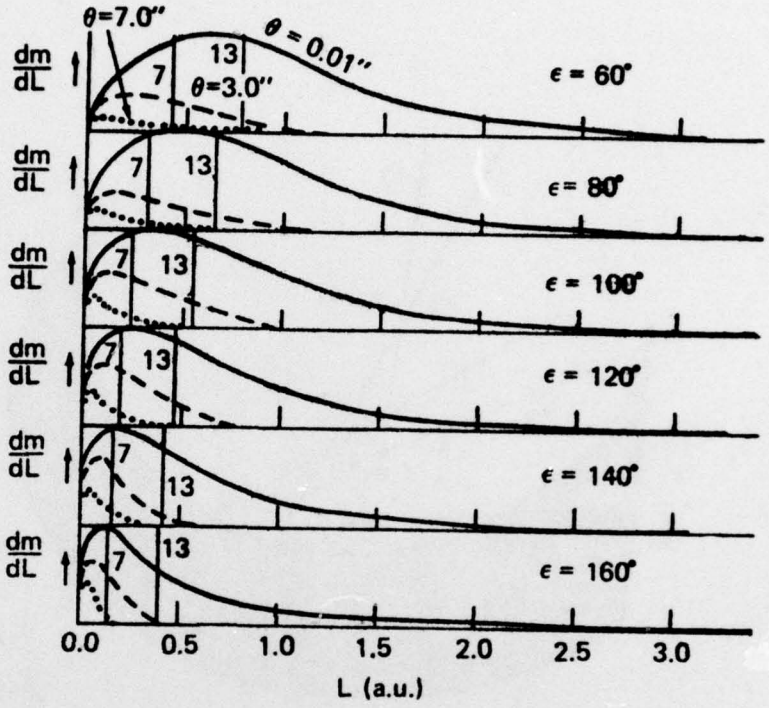


Figure 2 Contribution to the scintillation index (band-passed from 0.1 to 1.5 Hz) as a function of distance along the line of sight for three source angular diameters (θ). The calculation was done for $F_o \propto r^{-4}$, q = 3.6, solar wind velocity V = 400 km/sec, and 34.3 MHz.

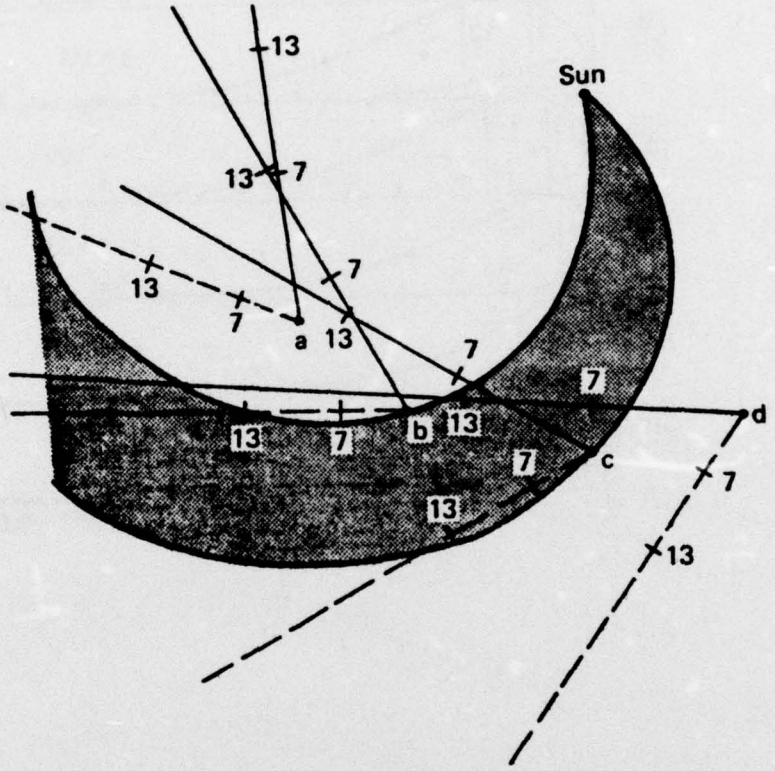


Figure 3 Geometry of a corotating turbulent region with various relative positions of the earth and the lines of sight to sources at 60° and 120° elongation. The locations of the centers of slabs 7 and 13 (of the total of 20) are indicated.

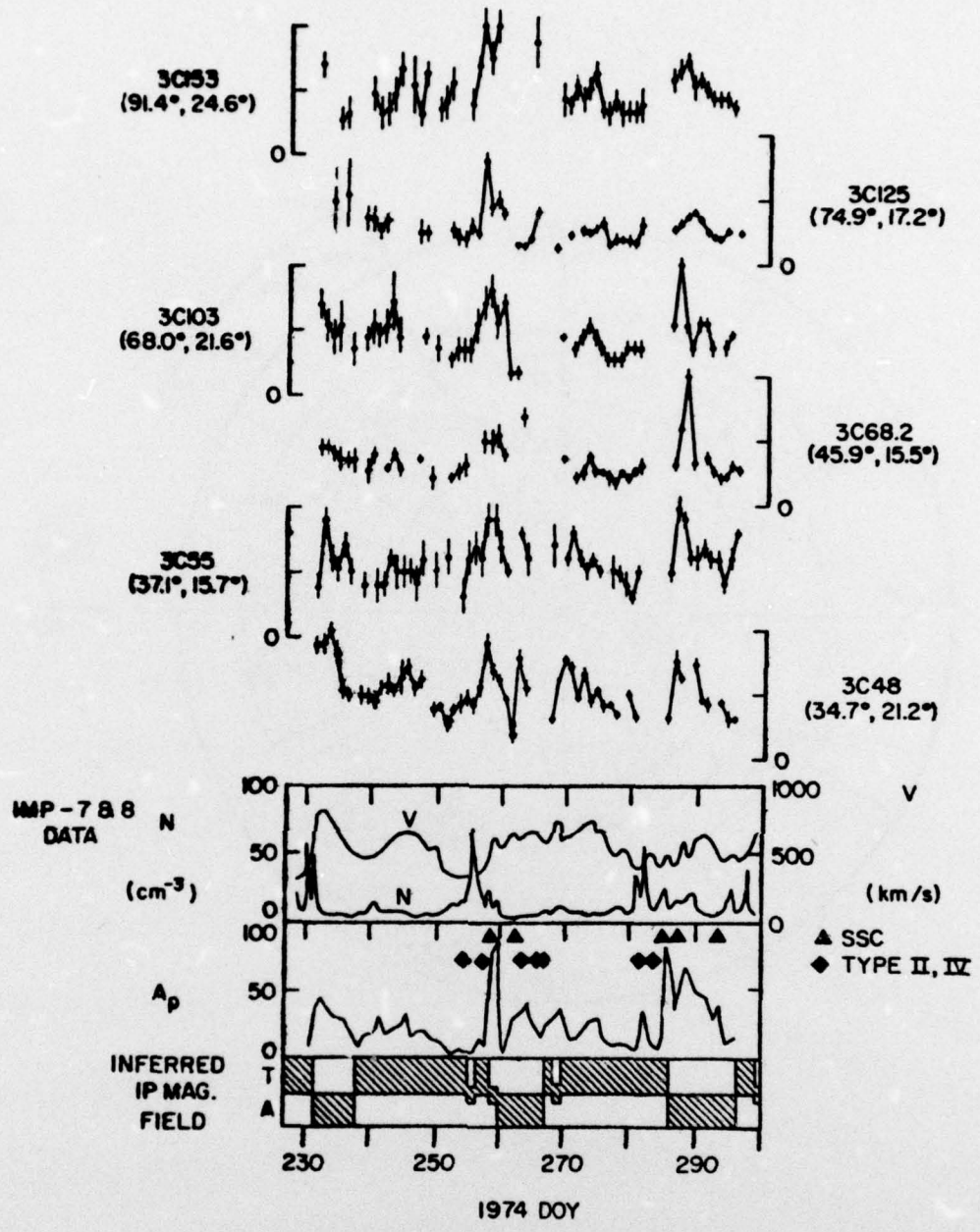


Figure 4 Synoptic observations of 6 scintillating sources in a region to the west of the sun of dimensions 9° (ecliptic latitude) by 57° (ecliptic longitude). Also shown are the following: IMP-7 and 8 solar wind proton density velocity (Los Alamos Scientific Laboratory); Geomagnetic $A_p$ index, and the occurrences of geomagnetic sudden commencements (SSC) and Type II and IV solar bursts in close association [Solar Geophysical Data]; and inferred interplanetary magnetic field direction [Svalgaard, 1975].

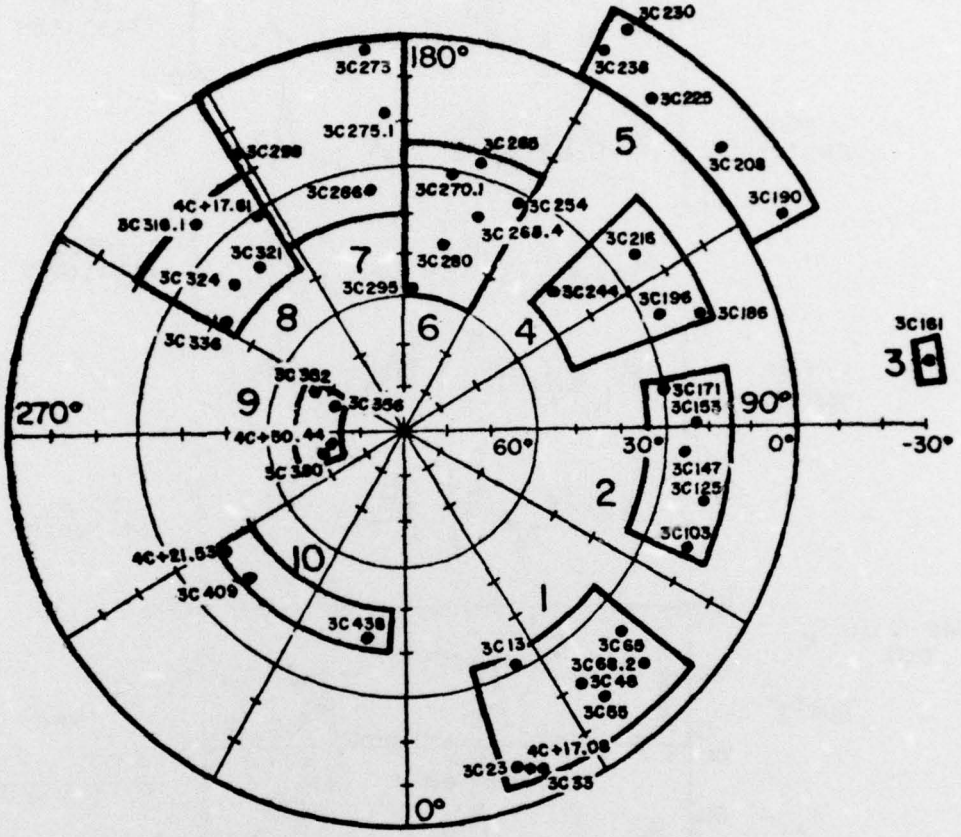


**Figure 5** Radio sources displaying usable IPS index during May-December 1974 clustered for IPS sky-box analysis. For this geocentric all-sky projection the azimuthal coordinate is ecliptic longitude relative to the Vernal Equinox (degrees) and the radial coordinate is ecliptic latitude (degrees).

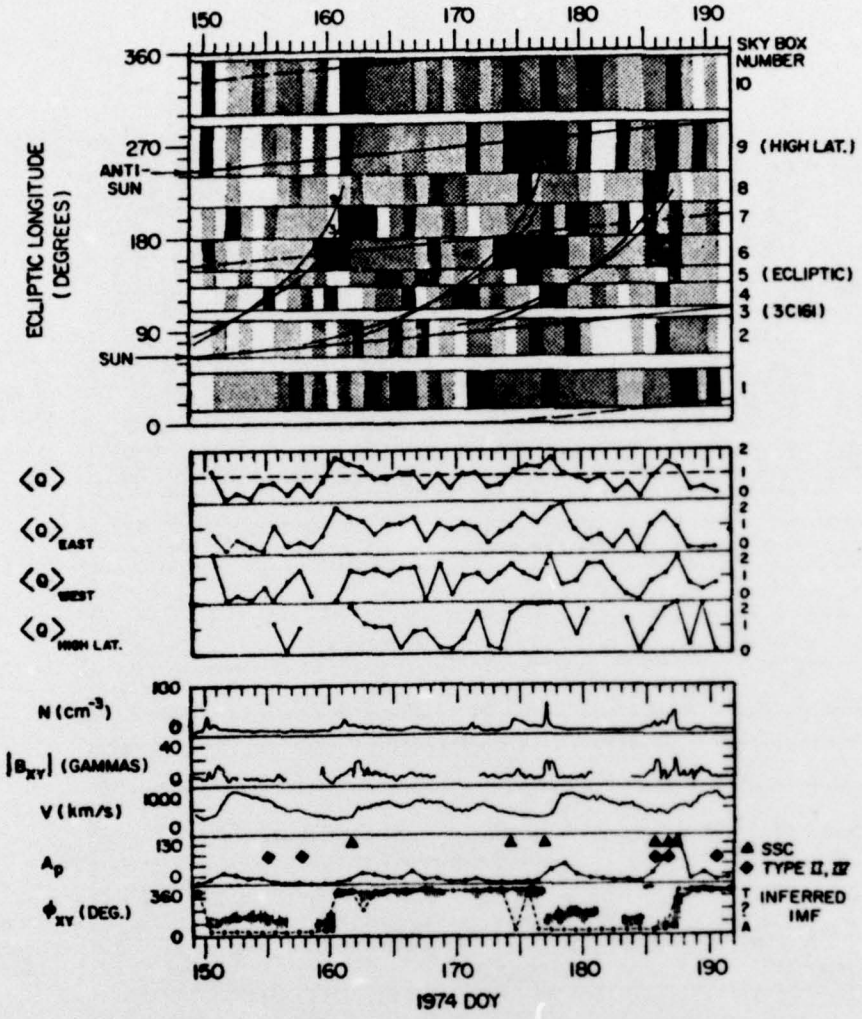


Figure 6 Results of radio source clustering analysis for 1974, days 150-190. Shading in each sky-box indicates high (dark shading), moderate (medium shading), low (light shading), or missing (no shading) IPS index. Heavy lines running diagonally in the body of the plot of ecliptic longitude vs. time represent the position of the sun and the direction 180° from the sun (anti-sun). Dashed lines running diagonally in body of each plot are drawn at 90° ecliptic longitude east and west of the sun. At the center are plots of IPS 'activity index' for the following cases: all 10 boxes averaged together, $< Q >$; eastern sky boxes only, $< Q >_{east}$; western sky boxes only, $< Q >_{west}$; high latitude box 9 only, $< Q >_{high\ lat.}$. At the bottom of the plot are the following correlative data: IMP-7 and 8 spacecraft solar wind proton density and velocity; interplanetary magnetic field magnitude $|B_{xy}|$ and solar ecliptic direction $\varphi_{xy}$; Geomagnetic $A_p$ index; inferred interplanetary magnetic field [Svalgaard, 1975] (dots with dashed lines).

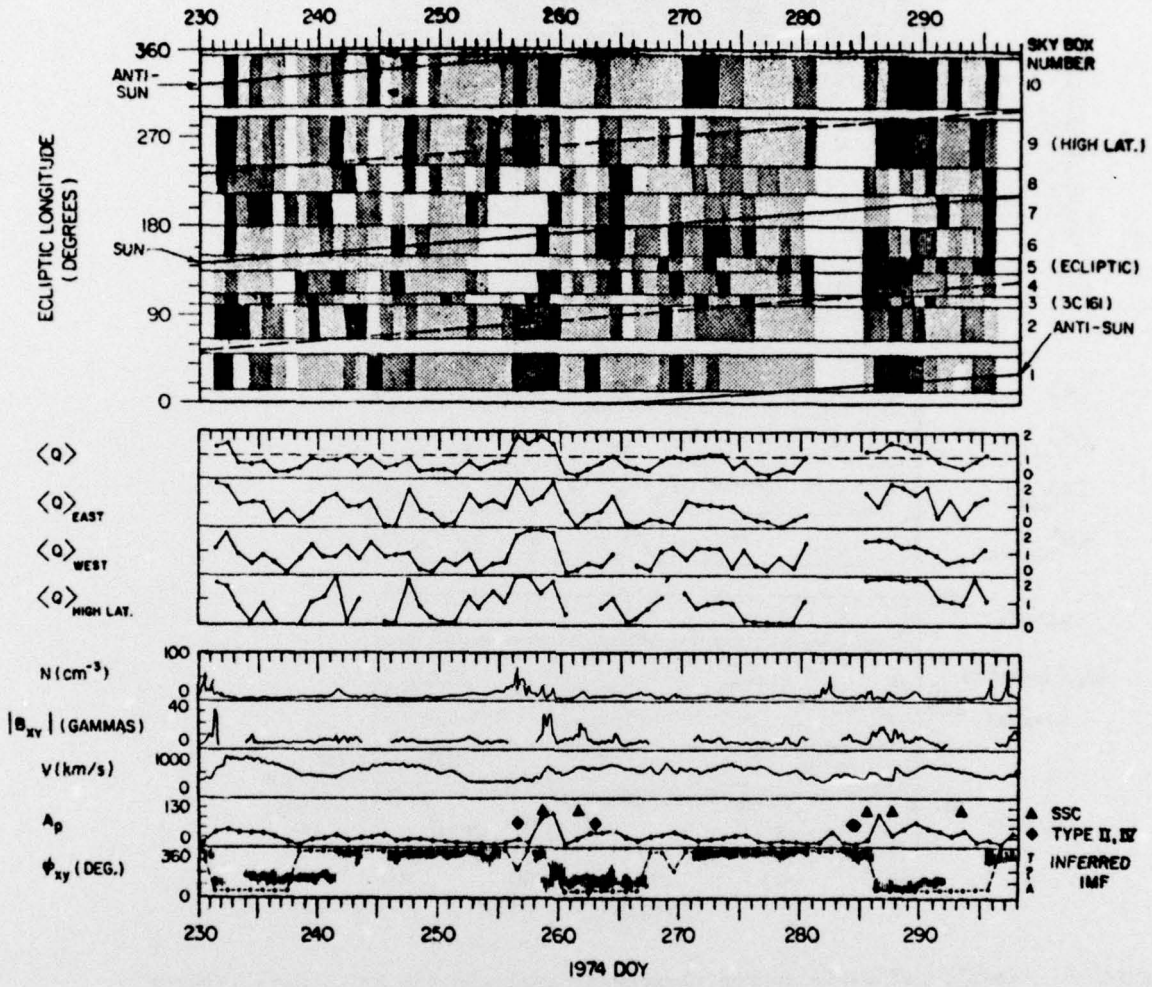


**Figure 7** Results of radio source clustering analysis for 1974, days 231-295. The format is the same as for Figure 5.

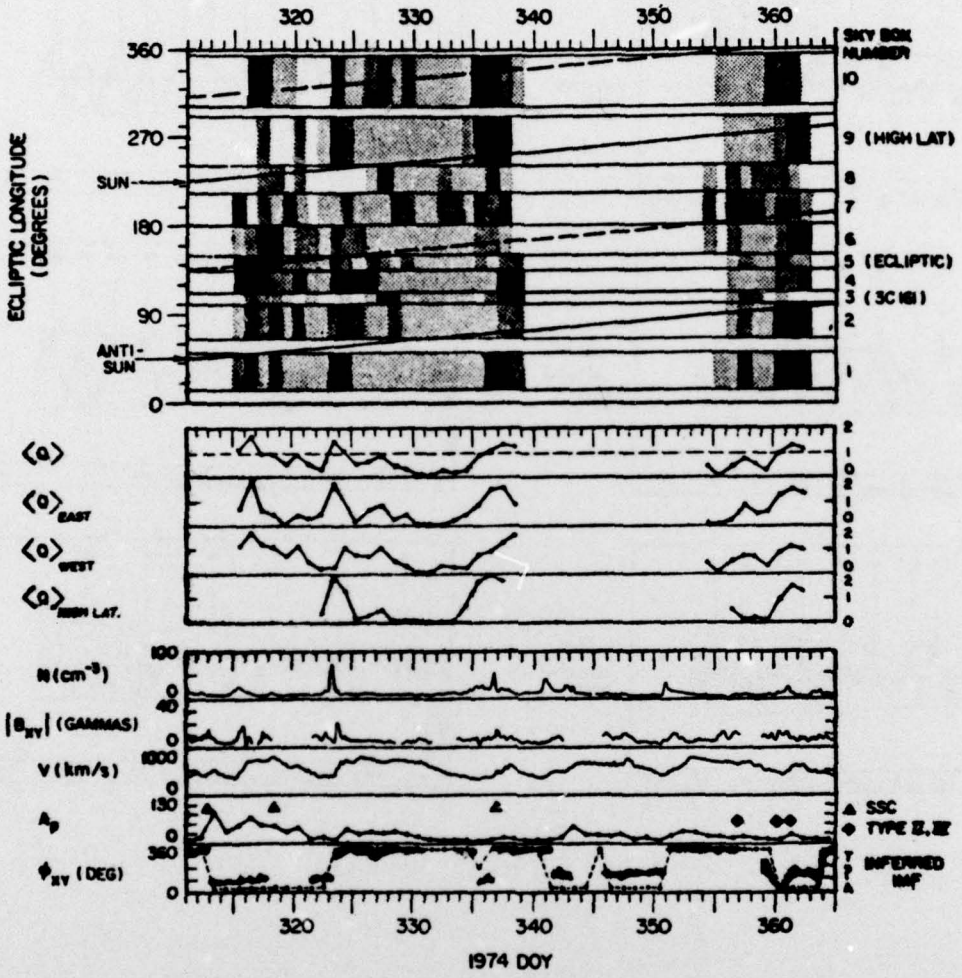


Figure 8 Results of radio source clustering analysis for 1974, days 315-362. The format is the same as for Figure 5.

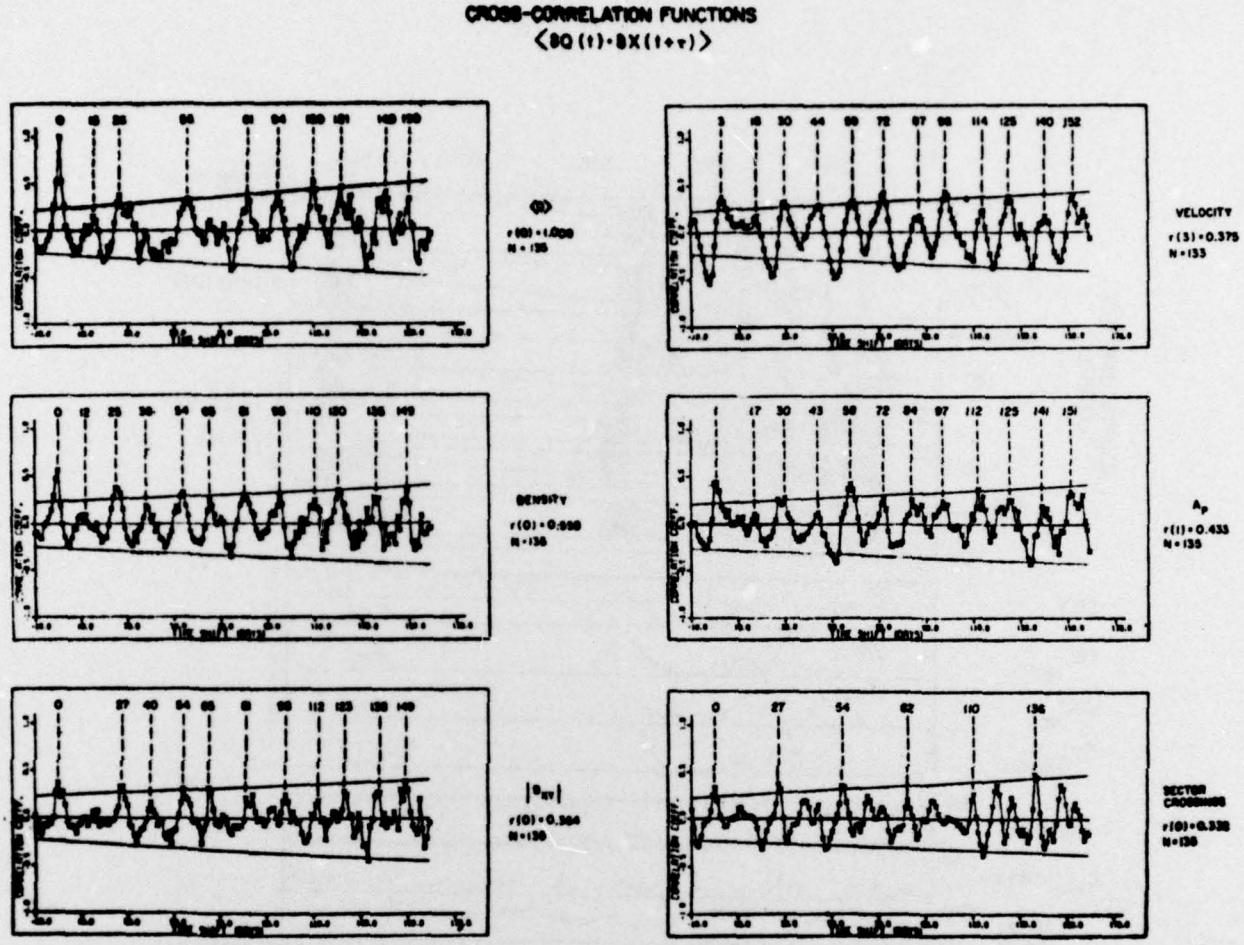


**Figure 9** Time series cross correlation results for correlation of all-sky IPS activity index' $< Q >$ versus the following' $< Q >$ (autocorrelation), solar wind proton density N, interplanetary magnetic field magnitude $|B_{xy}|$ (ecliptic projection), solar wind proton bulk velocity V, planetary geomagnetic A index, and occurrences of interplanetary sector crossings. Plotted is the crosscorrelation coefficient $r(\tau)$ for time shifts - 10 day $\leq \tau \leq$ 159 days. The data base is 1974, days 150-362. Also listed is $r(\tau)$ for the peak nearest $\tau \neq 0$ days, as well as the number of points, n, in the time series. The diverging lines indicate the 99% confidence limits.

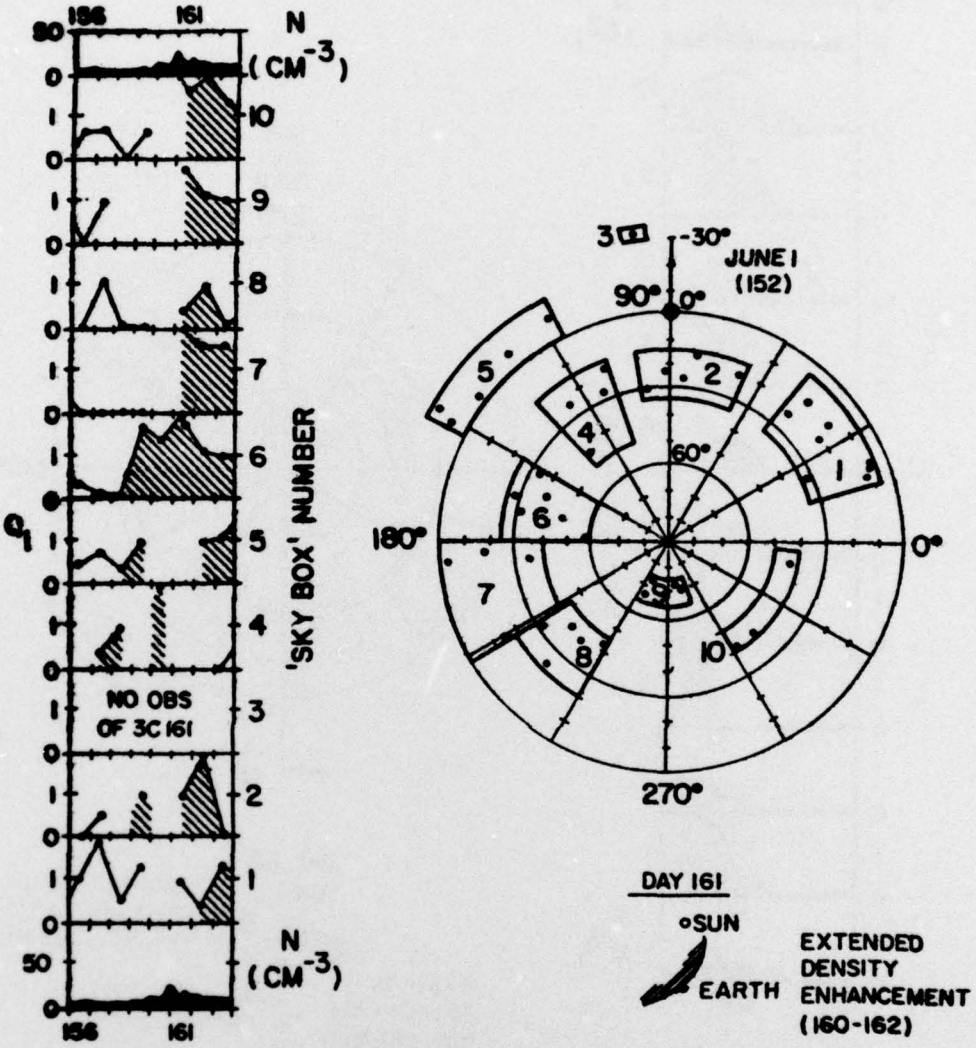


Figure 10 IPS 'sky box' analysis and solar wind density N for 'density event' of 1974, day 161.

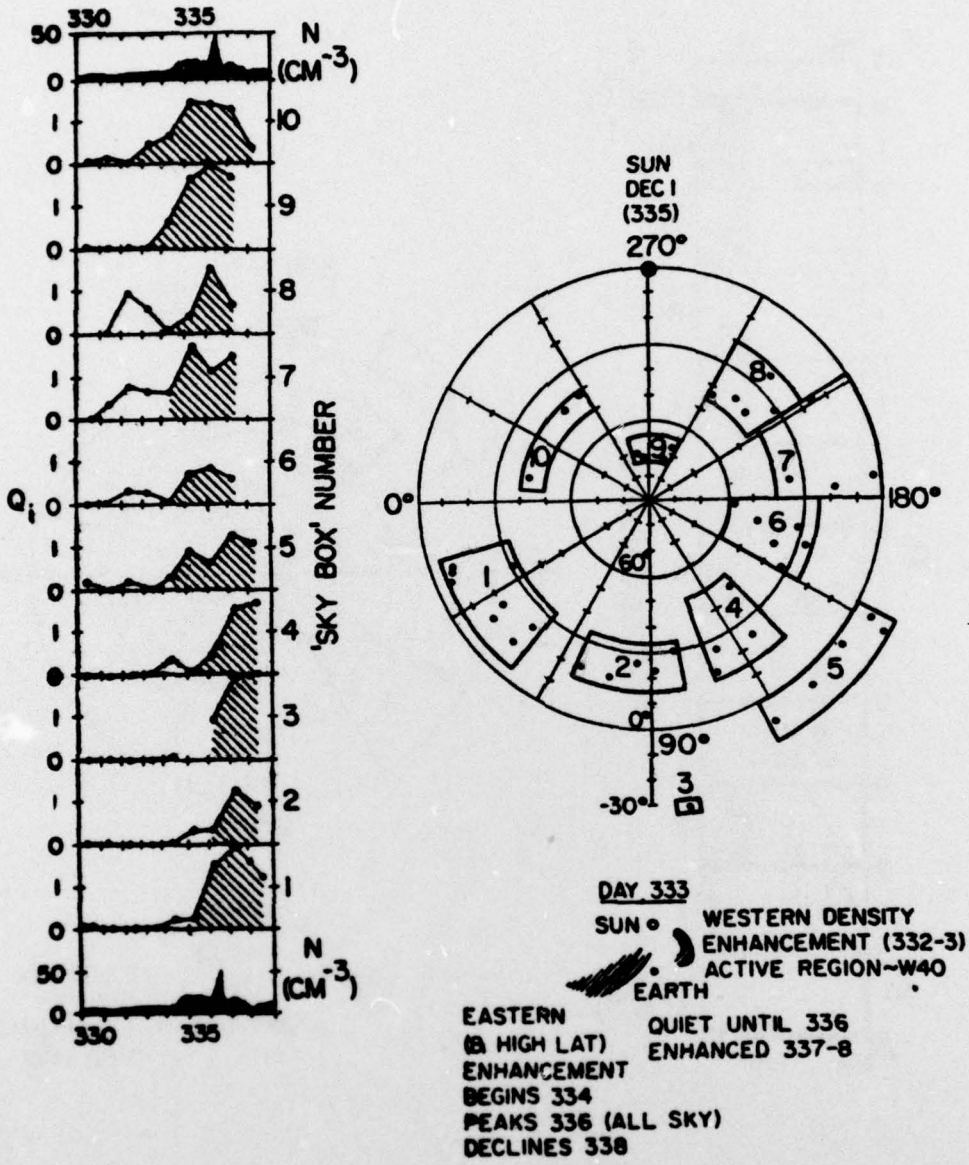


Figure 11 IPS 'sky box' analysis and solar wind density N for 'density event' of 1974, day 335.

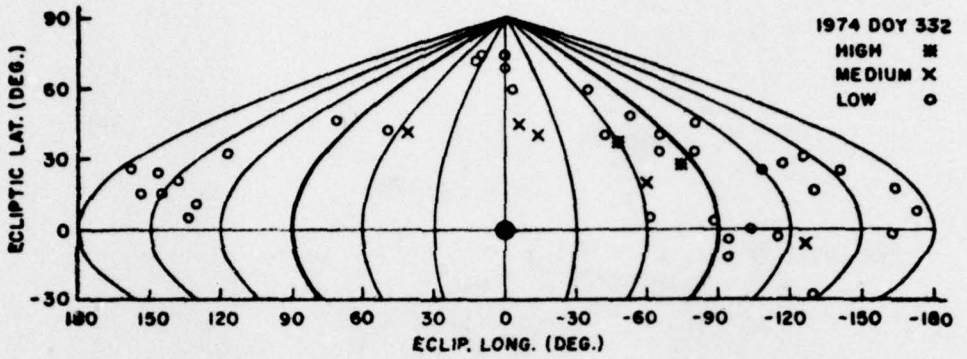


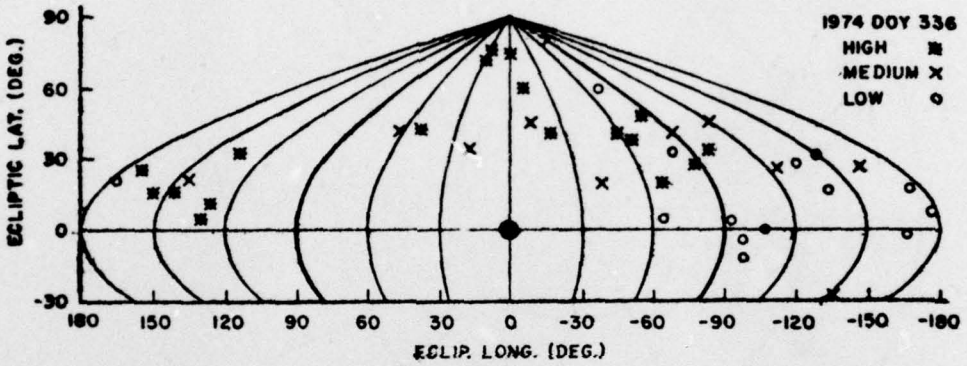


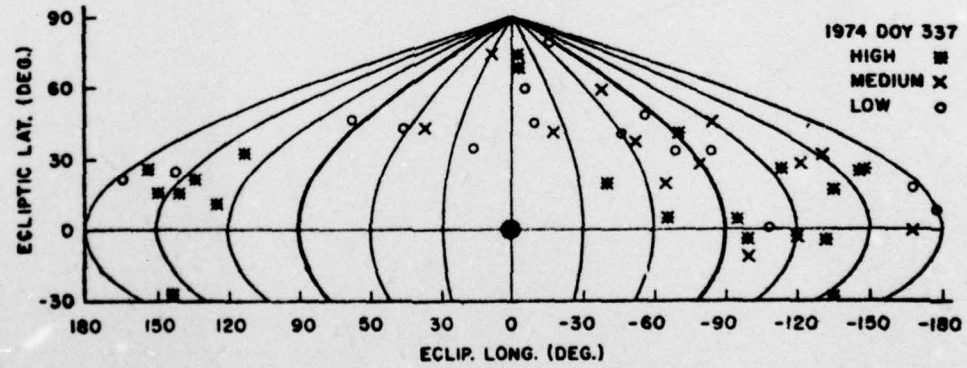


**Figure 12** Equal-area sky maps of IPS activity for 1974 a) day 332, b) day c) day 337.

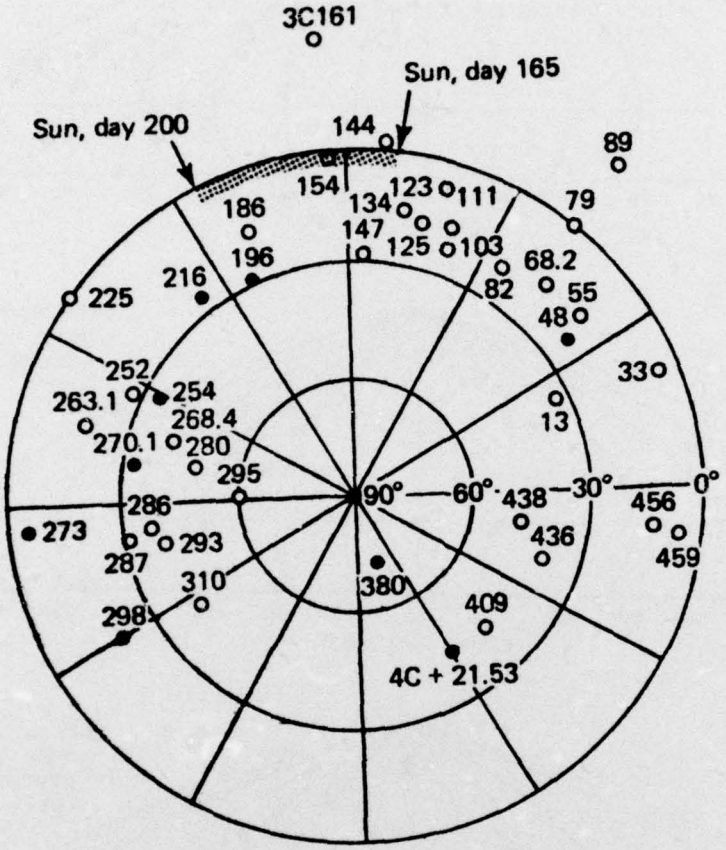


**Figure 13** Subset of 41 sources observed by the COCOA-Cross radio telescope. Sources plotted with a filled circle consistently yielded useful spectra.

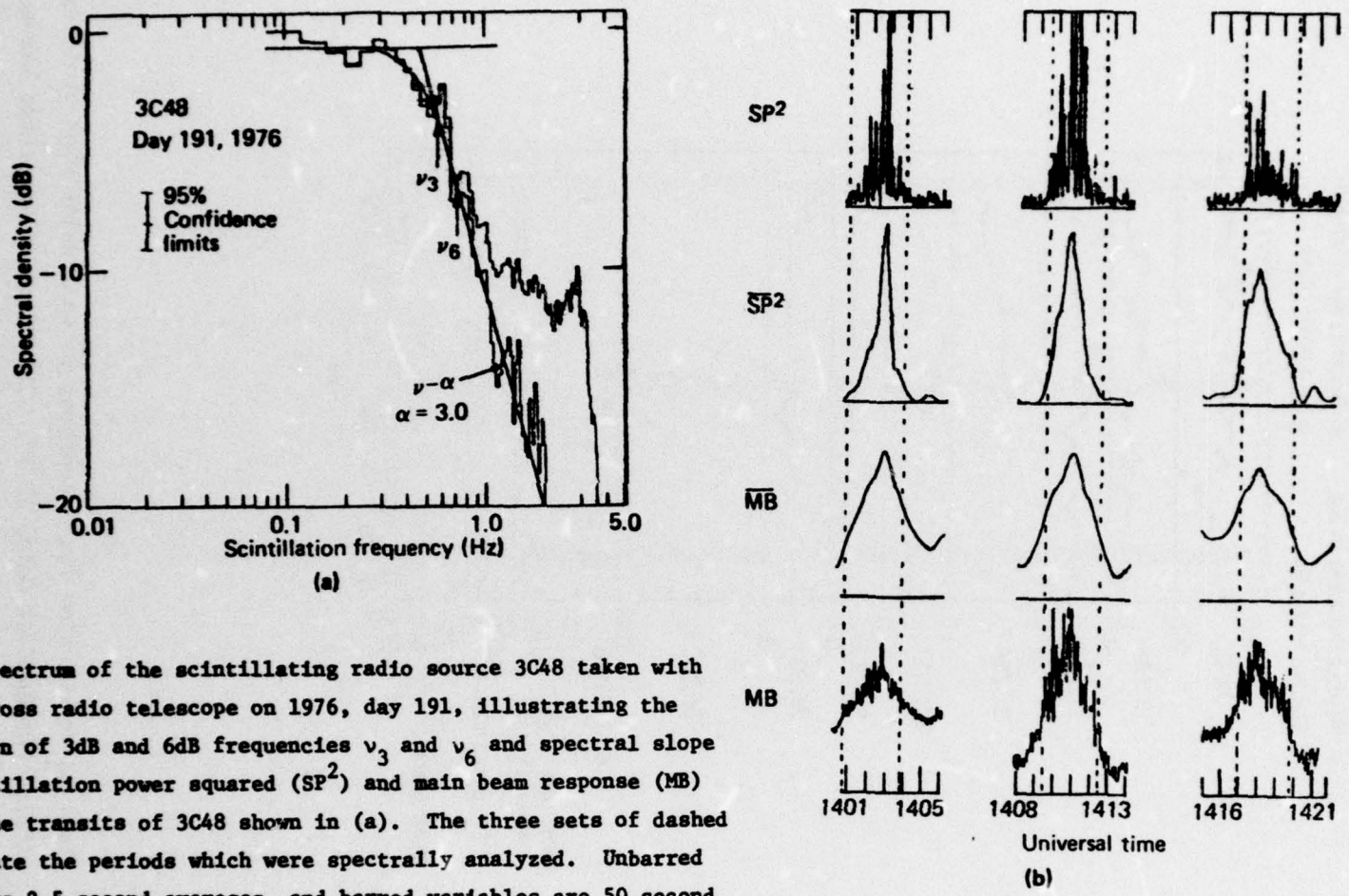


**Figure 14**

**(a) Power spectrum of the scintillating radio source 3C48 taken with the COCOA-Cross radio telescope on 1976, day 191, illustrating the determination of 3dB and 6dB frequencies $\nu_3$ and $\nu_6$ and spectral slope $\alpha$, (b) Scintillation power squared ($SP^2$) and main beam response (MB) for the three transits of 3C48 shown in (a). The three sets of dashed lines indicate the periods which were spectrally analyzed. Unbarred variables are 2.5 second averages, and barred variables are 50 second triangle weighted averages.**

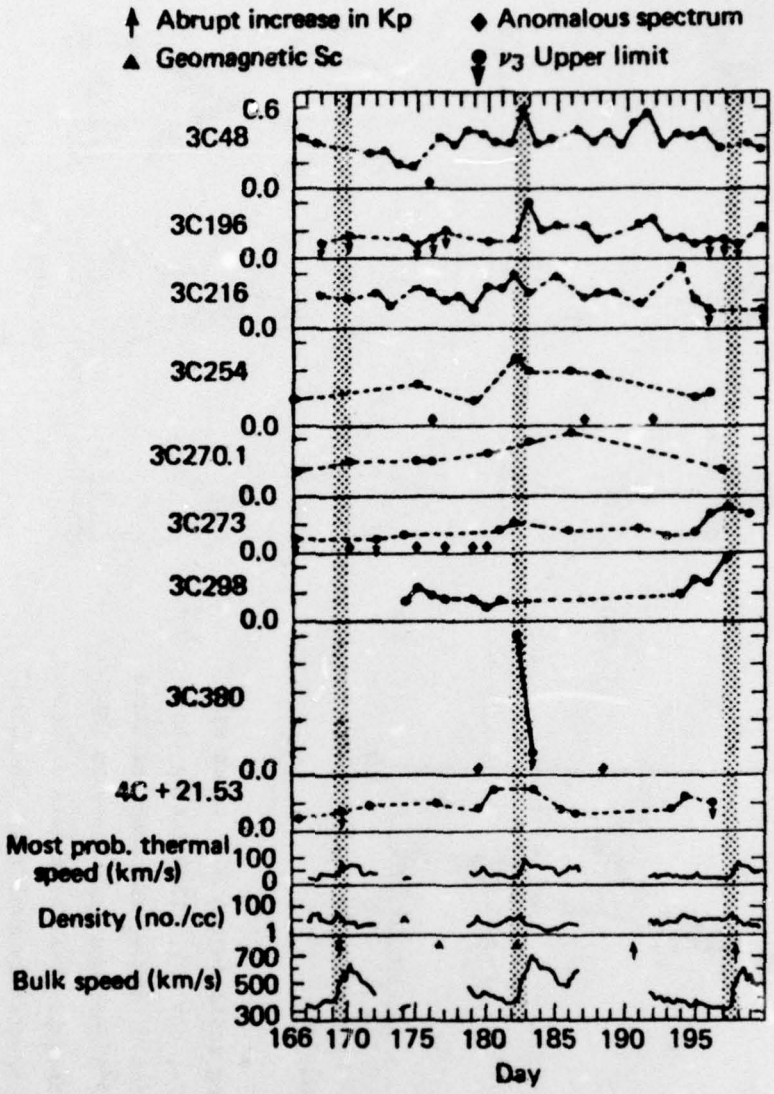


Figure 15 Top: $\nu_3$ versus time for 9 sources, Bottom: solar wind probe data *(Solar Geophysical Data, 1977)*. The start of the three known solar wind streams is highlighted by shading. On those days when a two component spectrum was present, or the spectrum was ambiguous, the data is omitted and a diamond is plotted near the bottom of the relavant curve.

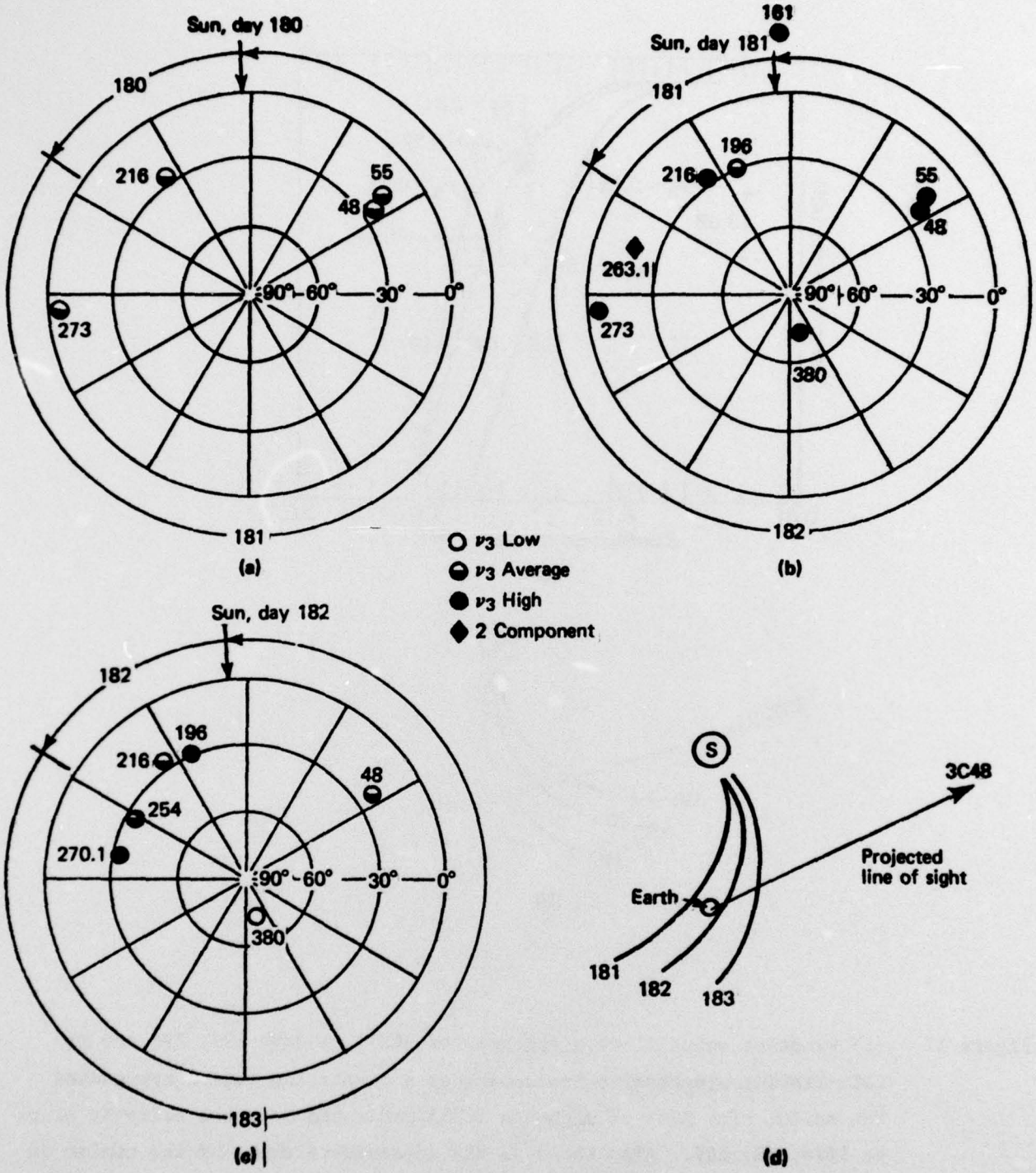


Figure 16 (a-c) $\nu_3$ for a number of sources, plotted in geocentric ecliptic coordinates. The "day cut" is at the sun, and the observations proceed in a counterclockwise sequence. The threshold for "low" and "high" is one standard deviation from the average. (d) Line-of-sight to 3C48 projected onto the ecliptic plane on 1976, day 182. Also shown is the approximate shape of the center of a corotating density enhancement for days 181, 182 and 183 at the time when 3C48 was observed.

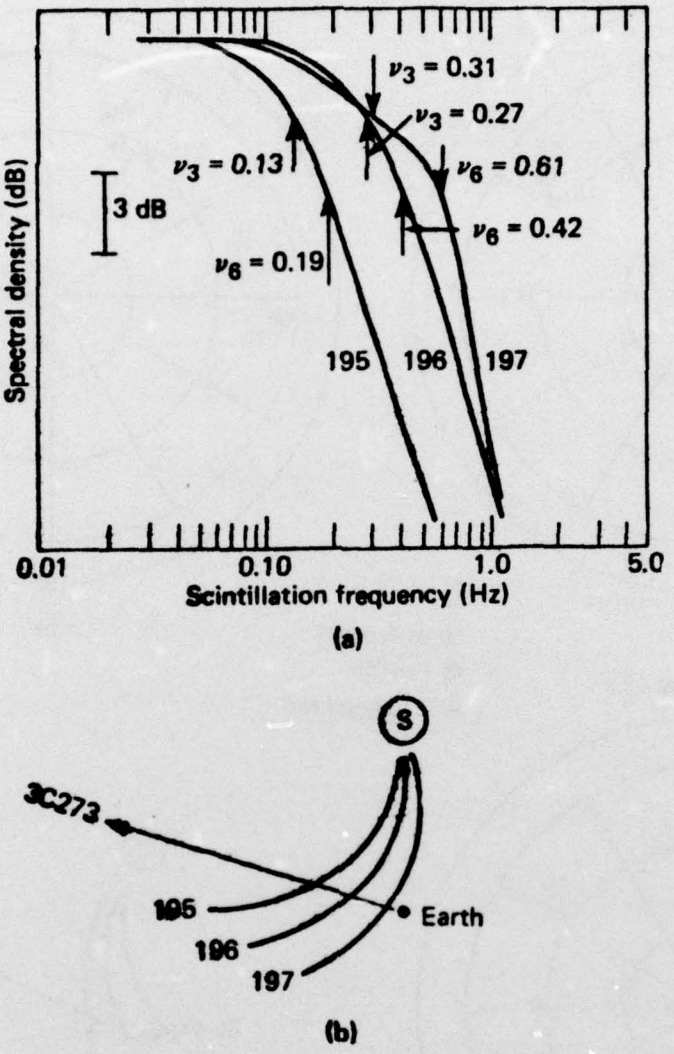


Figure 17 (a) Smoothed scintillation spectra for 3C273 on days 195, 196 and 197 illustrating progressive broadening as a corotating region approaches the earth. (b) Line of sight to 3C273 projected onto the ecliptic plane on 1976, day 197. Also shown is the approximate shape of the center of a corotating density enhancement for days 195, 196 and 197 at the time when 3C273 was observed.